The Role of Integrins in Cellular Response to Mechanical Stimuli

A thesis

Submitted to the faculty of the

WORCESTER POLYTECHNIC INSTITUTE

in partial fulfillment of the requirements for the Degree of

Master of Science

December 2016

Submitted by: Gawain M. Thomas

Department of Physics

APPROVED BY:

_____
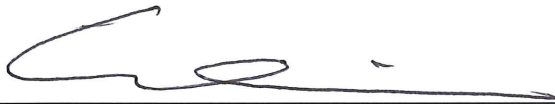
Dr. Qi Wen, Thesis Advisor

_____

Dr. Nancy A. Burnham, Committee Member

_____

Dr. Germano S. Iannacchione, Committee Member

Abstract

Tissue cells exhibit varying responses according to the stiffness of their extracellular matrix (ECM). The mechanism of this stiffness sensing is not fully understood; however, it is known that cells probe stiffness by applying intracellular force to the ECM via integrin-mediated focal adhesions. The bonds between integrins and ECM have been described as "catch bonds", and it is unclear how ECM viscoelasticity affects these bonds. We have observed the effects of ECM stiffness on the binding strength of integrins to ECM ligands by measuring the dissociation force of individual integrin-ligand bonds of 3T3 fibroblasts on collagen-coated polyacrylamide gels using atomic force microscopy. Results show that integrins exhibit higher rates of activation on stiff substrates. Furthermore, increased matrix stiffness results in the occurrence of larger, multi-bond dissociation events, which suggests that substrate stiffness may affect the cellular response by promoting integrin clustering as well as by modulating the maximum possible force between individual integrins and the ECM.

Acknowledgements

Table of contents

List of Figures

Chapter 1 – Introduction

Tissue cells respond in numerous ways to their surroundings. For example, it has been shown that tissue cells attached to a rigid surface such as bone or glass will spread to a larger area and exhibit a higher stiffness than the same cell type attached to a soft material. Depending on the stiffness of their surroundings, cells can also change their migratory patterns and rate of proliferation. This effect can be seen in **Figure 1**, from the work of Georges and Janmey [1]. Although the modulus values of the gels were not reported, the cell shape changes dramatically between soft and stiff polyacrylamide gel environments. In addition to the observed changes in cell morphology, we have observed changes in cell stiffness (Young's modulus) of up to two orders of magnitude [2] depending on the stiffness of the substrate, as measured by Atomic Force Microscopy (AFM). A detailed discussion of the measurement is made in Chapter 3.
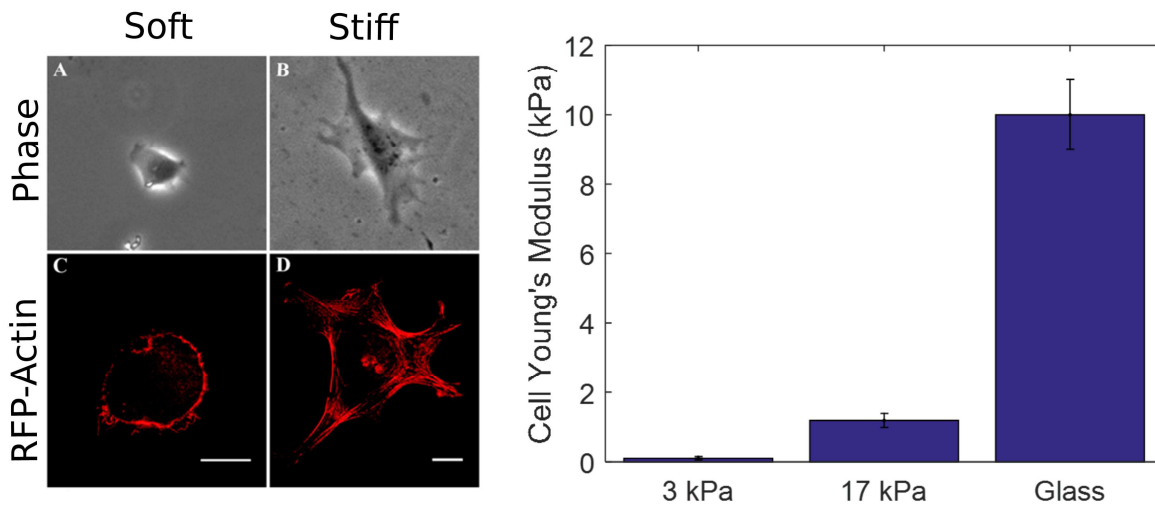
Figure 1. Effect of substrate stiffness on cell shape and stiffness.
 Left: Phase contrast images of NIH-3T3 fibroblasts on soft (A) and stiff (B) polyacrylamide gels. Actin staining shows no stress fibers in cells cultured on soft gels (C), and pronounced stress fibers on the edges of the cell cultured on stiff PA (D). Image excerpted from Ref. [1]. Right: Elastic modulus of NIH-3T3 fibroblasts measured using AFM on polyacrylamide gels of 3 kPa and 17 kPa, and on glass.

The cellular response to changes in external mechanical properties is thought to play some role in the progression of cancerous tissues. For example, if a healthy cell is in contact with a softer, cancerous tissue, this may reduce the healthy cell's structural stability leading to a reduction in

cell function and stiffness. Subsequently, other cells may respond in the same way, leading to a cascading effect of tissue degradation over large areas.

Why do cells respond like this?

Regulation of cell stiffness is driven by the tension of the cytoskeleton, which relies upon the anchoring of the cell to surrounding structural supports. The cytoskeleton consists of many complex molecular components, which include molecular motors, actin filaments, ligand receptors, microtubules, and others. Each of these components may exhibit different responses to mechanical and chemical cues from the environment. When the external stiffness changes, it affects the ability of each of these components to transmit force through the cytoskeleton, altering the cell's shape and mechanical properties.

In the following chapters, we will exercise an in-depth investigation of the role played by the integrins, which are a type of transmembrane receptor, in regulating the cellular response to mechanical stimuli. The integrins are embedded in the cell membrane, and form the mechanical link between extracellular ligands and the cytoskeleton. This investigation will make a modest contribution to a large body of research surrounding the interaction of cytoskeletal components with extracellular materials.

Chapter 2 – Background

Mechanotransduction and response to the cellular environment

Numerous studies have shown that tissue cells respond to the mechanical properties of their extracellular matrix (ECM) by adapting their own stiffness, morphology, and migratory behavior [3-9]. It remains unclear exactly what mechanism is responsible for this stiffness sensing. The underlying principle for stiffness measurements is a relatively universal one, beginning with the application of a force to the material, followed by an observation of the resulting deformation. Tissue cells generate intracellular force to deform the ECM by activating the molecular motors [10]. The path of force transmission includes cytoskeletal filaments such as F-actin, adapter proteins such as talin and vinculin, transmembrane proteins such as integrins, and the ECM ligands such as collagen and fibronectin [11-13]. The interactions between these components in the force propagation pathway can affect the efficiency of force transmission and hence the cell's sensitivity to ECM stiffness. For example, the linkage between the actin cytoskeleton and the integrins has been described as a slip clutch [14], which exhibits substrate stiffness-dependent changes in clutch dynamics. As the substrate stiffness is increased, the clutch behavior transitions from an oscillatory "load-and-fail" dynamic to a continuous frictional slippage, leading to changes in the rate of F-actin retrograde flow and the mean cellular traction force exerted on the substrate.

Cell-matrix adhesions are primarily mediated by integrins

In contrast to the extensive investigations on the intracellular components of the mechanotransduction pathway, the extracellular components – primarily the binding between cellular integrins and ECM ligands – have been minimally investigated in terms of their role in cellular mechanosensation and signaling. However, fundamental knowledge exists covering the process by which cells attach to the ECM, starting with the formation of single integrin-ligand bonds which then develop to form focal complexes and focal adhesions.

The structure of the ECM resembles a complex network composed of fibrous proteins, such as collagen, and other adhesive molecules including fibronectin, as well as proteoglycans [15, 16]. The architecture and composition of the ECM can vary widely between tissue types, and therefore the mechanical properties will be different depending on the tissue. For example, muscle tissue is more rigid than brain tissue, while being more compliant than skin or bone [8].

The stiffness of the ECM can play a significant role in determining cellular behavior, as discussed earlier. Cells exert a contractile force, known as a traction force, against the matrix, and cells on stiffer matrices are able to produce larger traction forces than on soft matrices [17], which may be due to the stiffer matrices' greater resistance to deformation. These different traction forces give rise to changes in various cellular characteristics including spreading area, motility, stiffness, and phenotype.

Integrins are a family of heterodimeric receptor proteins that reside within the cell membrane and bind directly to ECM ligands to initiate the formation of adhesions. These receptors are composed of α and β subunits. Altogether 18 α and 8 β subunits have been discovered in mammalian cells, which form 24 distinct integrins [18, 19]. The extracellular domain of the integrins binds to ECM proteins including collagen, fibronectin, laminin, and vitronectin as the integrins migrate along the cell membrane and cluster to form stronger adhesions. The cytoplasmic domains of the integrins are linked to the cytoskeleton by way of adaptor proteins which include talin, vinculin, paxillin, and α-actinin. 3T3 fibroblasts express several integrins, including α1β1, α2β1, α11β1, α6β1, α3β1, and α5β1 [20]. Of these, the most common integrin that has high affinity for collagen I is α2β1 [21].

The binding affinity of integrins to ligands can be regulated through a rapid and reversible process known as integrin activation. Chemical signaling pathways interact with the cytoplasmic domains of the integrins, altering the integrin's conformation, and subsequently inducing changes in the extracellular domains. These conformational changes can reveal or conceal cryptic binding sites, modulating the affinity for binding to a ligand. The two conformational states are illustrated in **Figure 2**.

In addition to the stimuli from within the cell (known as inside-out signaling, which results in changes integrin activation), integrins can also respond to external signals (outside-in signaling, in which a mechanical stimulus is transmitted through the cytoskeleton). As an example of outside-in signaling, a twisting force applied to β_1 integrins resulted in the formation of focal adhesions and stiffening of the cytoskeleton in direct proportion to the applied force [22]. The ability of integrins to transmit signals bi-directionally in and out of the cell makes them a critical component in mechanotransduction and signaling.
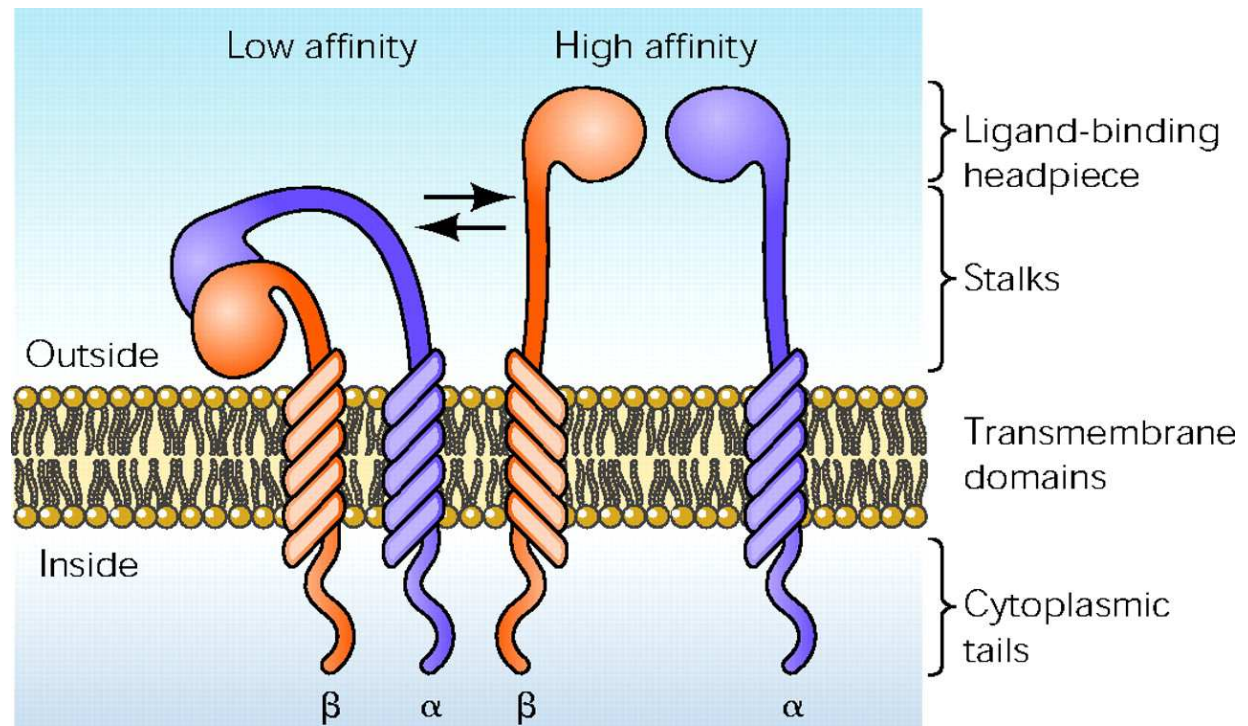
Figure 2. Heterodimeric structure of the integrins[23]. Left: Unbound integrins normally reside in the low-affinity (non-activated) state. Right: Under applied tension, the integrin switches to the "active" conformation, revealing cryptic binding sites and increasing the ligand binding affinity.

Development of the adhesion complexes

Following the initial binding of an integrin to an ECM ligand, the adhesion site undergoes several stages of strengthening, which have been studied extensively [8, 15-19, 22, 24, 25]. First, the binding of integrins to ligands leads to integrin clustering, followed by the recruitment and activation of enzymes such as tyrosine. As time passes, the cluster of integrins may develop into larger structures known as focal complexes and focal adhesions. The structure of the integrin clusters is illustrated in **Figure 3**.
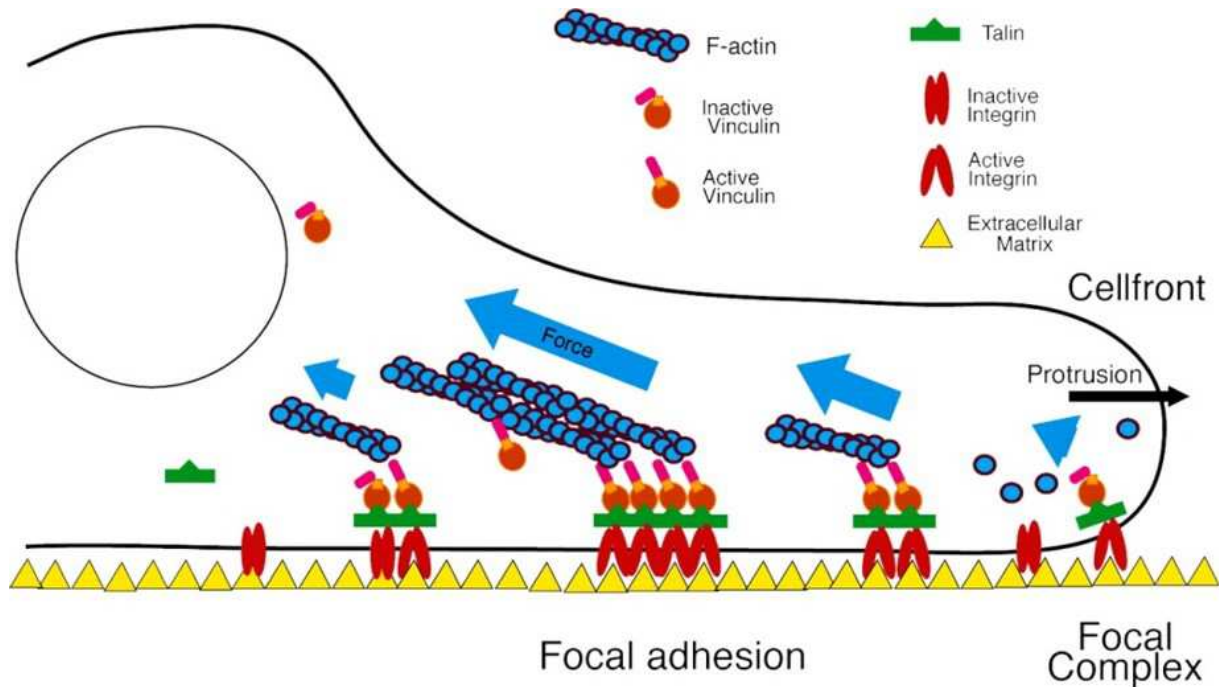
Figure 3. Illustration of cellular adhesions [26]. Initially, a single integrin binds to the ECM and is activated by force from the cytoskeleton. Activation of the integrin leads to chemical signaling that recruits additional integrins to form a focal complex, which then matures into a focal adhesion.

Focal Complexes

Focal complexes are small adhered patches (~1 μm^2 or smaller) typically localized near the lamellipodium edge of the cell [27]. The existence of a focal complex is characterized by the colocalization of integrins, talin, vinculin, paxillin, Focal Adhesion Kinase (FAK), and phosphotyrosine [15]. The formation of focal complexes can be promoted by the application of force [28] to the integrins, and it has been shown that integrin clustering is increased on stiff matrices[17]. Because early integrin-cytoskeleton linkages are reinforced in proportion to the applied force, the rigid substrates promote greater strengthening of focal adhesions than compliant matrices due to greater resistance to deformation and subsequently larger forces.

Because the cryptic vinculin binding sites on talin are exposed during stretching of the talin molecule, the localization of vinculin at the adhesion site increases under force. Vinculin, in turn, induces actin cytoskeletal reorganization which can increase the traction force generated by the cell [29]. This is a direct example of how tension applied during focal complex formation leads to increased traction force, and consequently increased cell spreading area and stiffness.

Focal Adhesions

During the transition from focal complexes into focal adhesions, the morphology of the adhesion site changes from a spatially symmetric spot to an elongated, polar formation with a "heel" and "toe" end, and newly formed actin bundles grow from the heel end. This transition is regulated by the Rho-family GTPase Rac [30]. Additionally, the application of force to the adhesion site can trigger actin and myosin to be assembled into stress fibers, which exert cytoskeletal tension, and in turn triggers the growth and elongation of the focal adhesion [17, 31].

Cells on stiff substrates form stable focal adhesions and have increased traction force and expression of integrins and stress fibers. Cells on soft matrices, however, form dynamic adhesions which allow for less spreading and faster migration [32]. A model has been proposed which suggests that the size and formation timescale of focal adhesions is proportional to the matrix stiffness, with small focal adhesions forming rapidly on soft matrices [33].

The behavior of individual integrin-ligand bonds

As previously discussed, the formation of cell-ECM adhesions and focal complexes are in large part initiated by the integrins binding to their respective ligands. The formation, strength, and lifetime of these initial bonds are dependent upon a set of binding affinities and reaction rates, which are dependent upon the intermolecular forces. George Bell proposed a model in the late 1970s [34] which postulated that the binding rate of integrins to ligands is dependent on attractive and repulsive forces due to osmotic, electrostatic, and other non-specific interactions, and that applying an external force to the bond will therefore affect the rate of dissociation. This phenomenon has been observed experimentally, for example, when the dissociation rate of zyxin increased in response to reduced traction forces [35] regardless of whether the reduction in traction force was achieved by altering matrix stiffness, inhibiting cell contractility, or directly cutting stress fibers.

In contrast to the intuitive prediction that a bond should fail more rapidly under applied tension, thermodynamics-based models have also predicted the existence of "catch bonds" which have increased strength when loaded [36]. These catch bonds have been demonstrated using AFM in a study that showed bonds between the $\alpha_5\beta_1$ integrin and fibronectin have longer lifetimes when

10-30 pN forces are applied, as a result of force-induced changes in the headpiece of the integrin [37].

The bond dissociation rate does not only depend upon the magnitude of force applied, however. Bond strength is dependent upon the rate and duration of loading, implying that the timescale of loading is important to the bond mechanics [38]. On the basis of Bell's model, the dissociation rate of receptor-ligand bonds increases exponentially with the externally applied force, as

$$v(F) = v_0 \exp\left(\frac{Fx_b}{k_BT}\right),$$

where k_BT is the thermal energy, x_b is the half-width of the bond's potential energy barrier (**Figure 4**), and v_0 represents the intrinsic dissociation rate of the bond under no load. Within a small time interval $(t, t + dt)$, the probability of bond dissociation is expressed by

$$P_d(t) = \alpha v(F) \exp\left\{-\int_0^t v(F(t'))dt'\right\},$$

where α is a normalization constant. When evaluated at a constant loading rate, $\dot{F}$, with $F(t) = \dot{F}t$, the probability can be expressed as a function of force alone:

$$P_d(F) = \alpha v_0 \exp\left(\frac{Fx_b}{k_BT}\right) \exp\left\{-\frac{v_0 k_BT}{x_b\dot{F}}\left(\exp\left(\frac{Fx_b}{k_BT}\right) - 1\right)\right\}.$$

By maximizing this dissociation probability, it is possible to determine a maximally probable dissociation force,

$$F_d = \frac{k_BT}{x_b}\ln\left(\frac{rx_b}{v_0 k_BT}\right),$$

where $r = \frac{dF}{dt}$ denotes the instantaneous external loading rate. The logarithmic dependence of F_d on the loading rate implies that not only is the bond strength sensitive to the loading rate, but the degree of sensitivity changes depending on the timescale of loading.
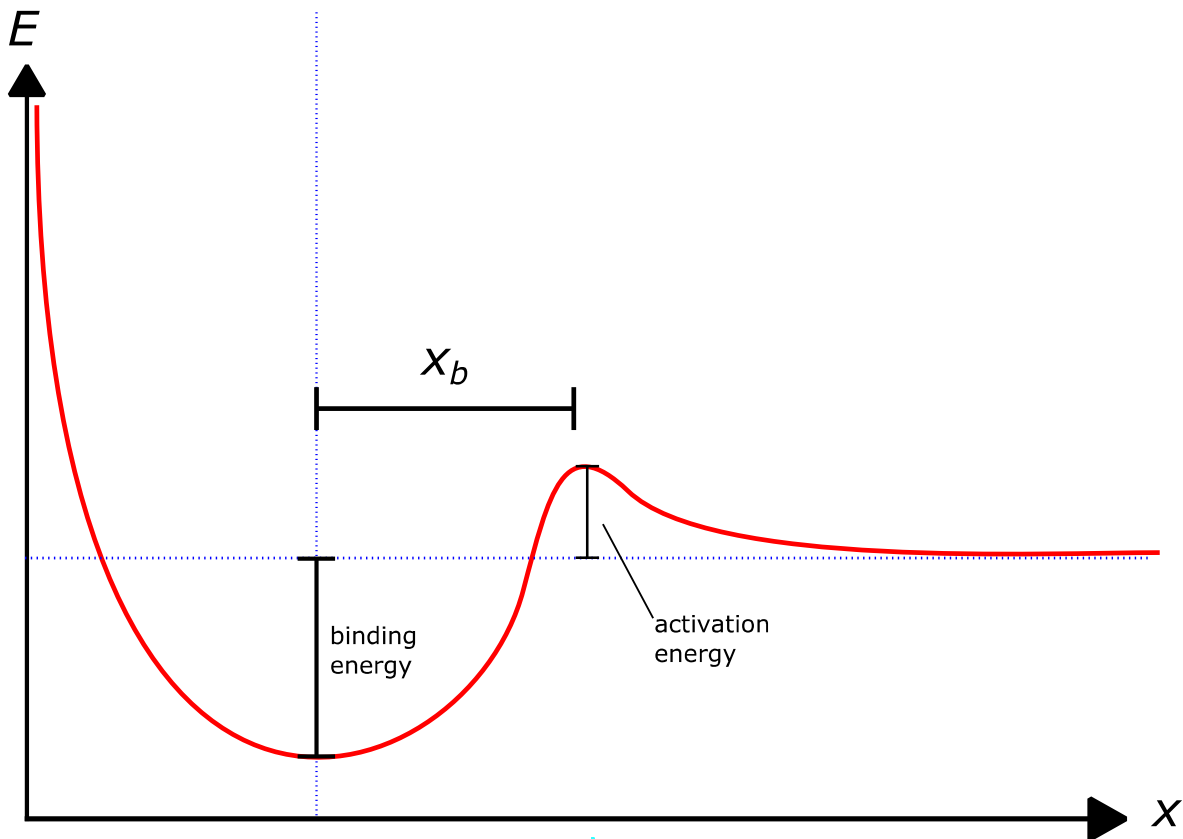
Figure 4. Energy landscape of the bond. The width parameter x_b represents the distance between the potential energy minimum and the activation barrier. The width and depth of the potential well depend primarily on the activation state of the receptors.

Evans and Ritchie [38] have produced molecular dynamics simulations which show that three principal regimes of loading exist, corresponding to different relationships between the loading rate and bond strength. Under slow loading, bond strength is practically constant and independent of the loading rate, as the unbinding is primarily a stochastic Brownian process. At intermediate speeds, the unbinding starts to be driven by the externally applied force, and bond strength increases logarithmically with loading rate. At fast loading rates, the bond strength reaches a plateau as the molecules are only held together by frictional forces. The three regimes are indicated in **Figure 5**. Quantifying the precise conditions that mark the transition between these regimes is nontrivial, and is dependent upon the model of molecular damping, the type of bonding potential, and spatial dimensionality. Therefore the critical rates that arise in simulations

cannot be directly compared to laboratory force-probe measurements. Still, the three regimes are representative of real physical phenomena that can be observed in the laboratory.
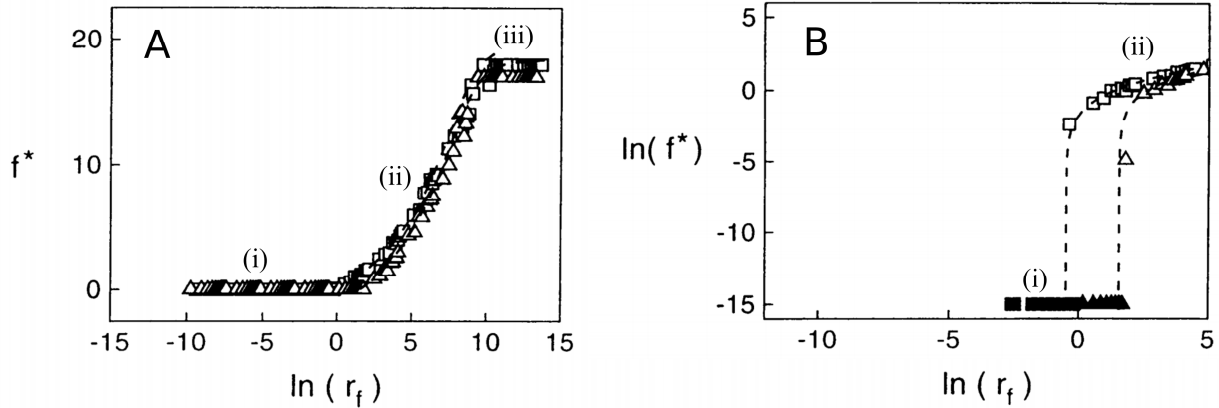
Figure 5. Three regimes of bond strengthening under load. (A-B) Images excerpted from [38] show that for small loading rates (i) there is no dependence of bond strength, f*, on the loading rate; at intermediate loading rates (ii) the bond strength increases logarithmically, and at high loading rates (iii) the bond strength cannot increase further. (B) Plotting log(f*) vs. log(r) shows a sharp transition from the loading-independent regime to the loading-dependent regime

ECM mechanics may affect receptor-ligand interactions

Because the rate of loading is correlated with the expected strength of integrin-ligand bonds, every component of the cell-receptor-matrix system will make some contribution in determining the bond rupture force. It may be instructive to depict the system as a set of Hookean springs in series, with separate springs representing the matrix, receptor-ligand bond, and, depending on the degree of model complexity, one or more components of the cell (**Figure 6**). It is common in studies of cellular adhesion and traction force to model the substrate and integrin-ligand bonds as in this way [39, 40].
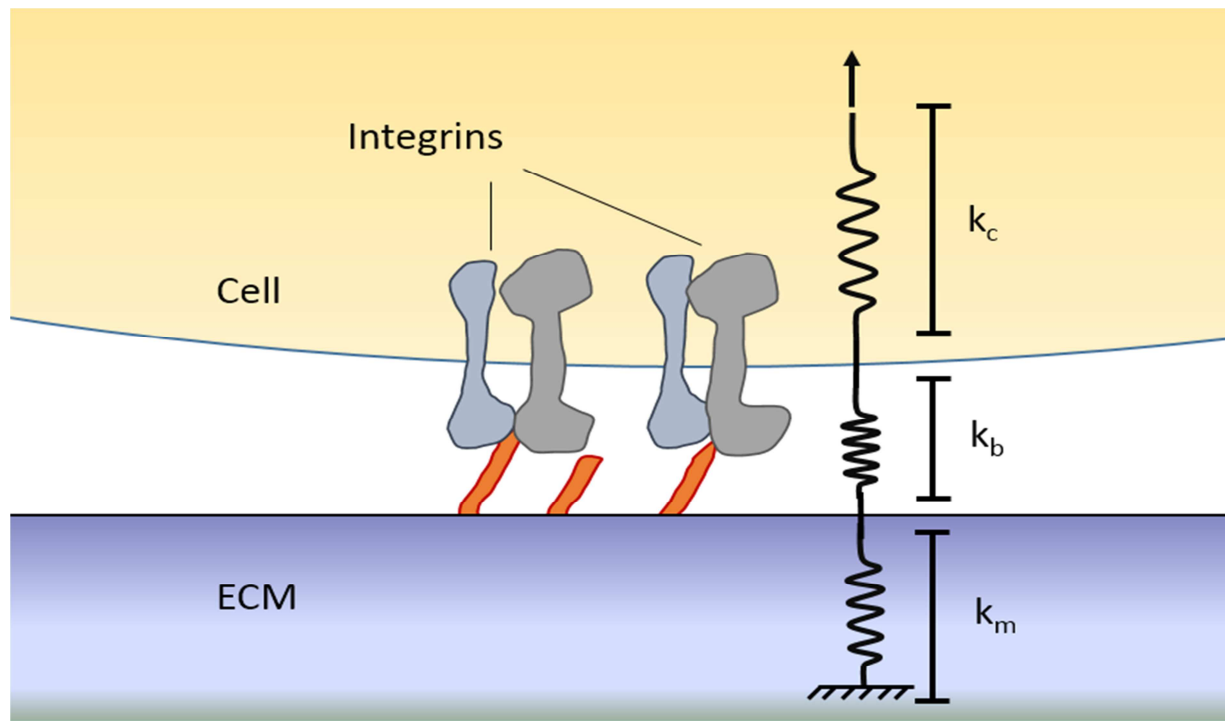
Figure 6. The components of the force propagation pathway can be modeled as springs in series. k_c, k_b, and k_m represent effective spring constants of the cell, integrin-ligand bond, and extracellular matrix, respectively.

Although this is a crude representation of the true biological system, it can nevertheless elucidate the role that mechanical properties of each component play in the loading and subsequent dissociation of the bond. For instance, if the cell is pulled away from the ECM at a constant velocity, $\Delta x/\Delta t$, then the tensional force felt by the bond will increase at a rate

$$\frac{\Delta F}{\Delta t} = \frac{\Delta x/\Delta t}{1/k_c + 1/k_b + 1/k_m}$$

which is dependent upon the mechanical properties of each component.

Chapter 3 –Measuring the stiffness of cells using AFM

Measuring cell elasticity and viscoelasticity

Multiple methods, including particle-tracking microrheology [41-44], magnetic twisting cytometry [45], micropipette aspiration [46], and microindentation [47-49] have been developed to measure the elasticity of cells. Particle tracking microrheology traces the thermal vibrations of either submicron fluorescent particles injected into cells or fiducial markers inside the cell cytoskeleton [50], and is capable of measuring particle displacements of 20 nm and larger [44]. Elastic and viscous properties of cells are calculated from the measured particle displacements using the fluctuation-dissipation theorem [42, 50]. This method allows simultaneous measurement of local mechanical properties with high spatial resolution at different places in a cell. However, injecting fluorescent particles into cells may lead to changes in cellular function, cytoskeleton structure, and hence the cell mechanics. The micropipette aspiration method applies negative pressure in a micropipette of diameter ranging from 1 to 5 μm to suck a small piece of cell membrane into the pipette. Cell stiffness is calculated from the applied negative pressure and cell membrane deformation [46]. This method, however, cannot detect the heterogeneous distribution of stiffness across the cell. Magnetic twisting cytometry applies magnetic field to generate torque on super paramagnetic beads attached to the cell membrane [45]. Cell stiffness is derived in this method from the relationship between the applied torque and the twisting deformation of the cell membrane. It is difficult to control the location of magnetic beads in the magnetic twisting cytometry method, and it is also challenging to characterize the twisting deformation with high resolution. Microindentation applies an indenter with well-defined geometry to punch into the cell. The indenting force and the resulting indentation in cells often follow the prediction of the Hertz model. Young's moduli of cells can be calculated from the force-indentation curves by fitting them to the Hertz model. The microindentation method has its own limitations, including time restrictions, uncertainty in contact point determination, and the potential to physically damage the cells. However, these limitations are ostensibly much less restrictive than those of the methods listed above. Although many other indenting devices have been developed [47], the Atomic Force Microscope (AFM) has been applied as a popular method to characterize mechanical properties of living cells and tissues [48, 51-54].

Here we demonstrate the procedure of using an Asylum MFP3D-Bio AFM to characterize cell mechanics. AFM not only provides high-resolution topography of cells but also has been widely applied to characterize the mechanical properties of tissue cells. The principle of AFM indentation is illustrated in **Figure 7**. The AFM cantilever approaches the cell from a few micrometers above; makes contact with the cell; indents the cell so that the cantilever deflection reaches a preselected set point; and pulls away from the cell. During this process the cantilever deflection is recorded as a function of its location as shown in **Figure 7**. Before making contact with the cell, the cantilever moves in the medium without any apparent deflection. When indenting on the cell, the cantilever bends and the deflection signal increases. The cantilevers are modeled as elastic beams so that their deflection is proportional to the force applied to the cell. By setting the maximum cantilever deflection, the maximum magnitude of force applied to the sample is limited to avoid damage to cells. The portion of the force curve from point b to point c in **Figure 7**, where the tip indents into the cell, is fit to the hertz model to extract the cell stiffness.
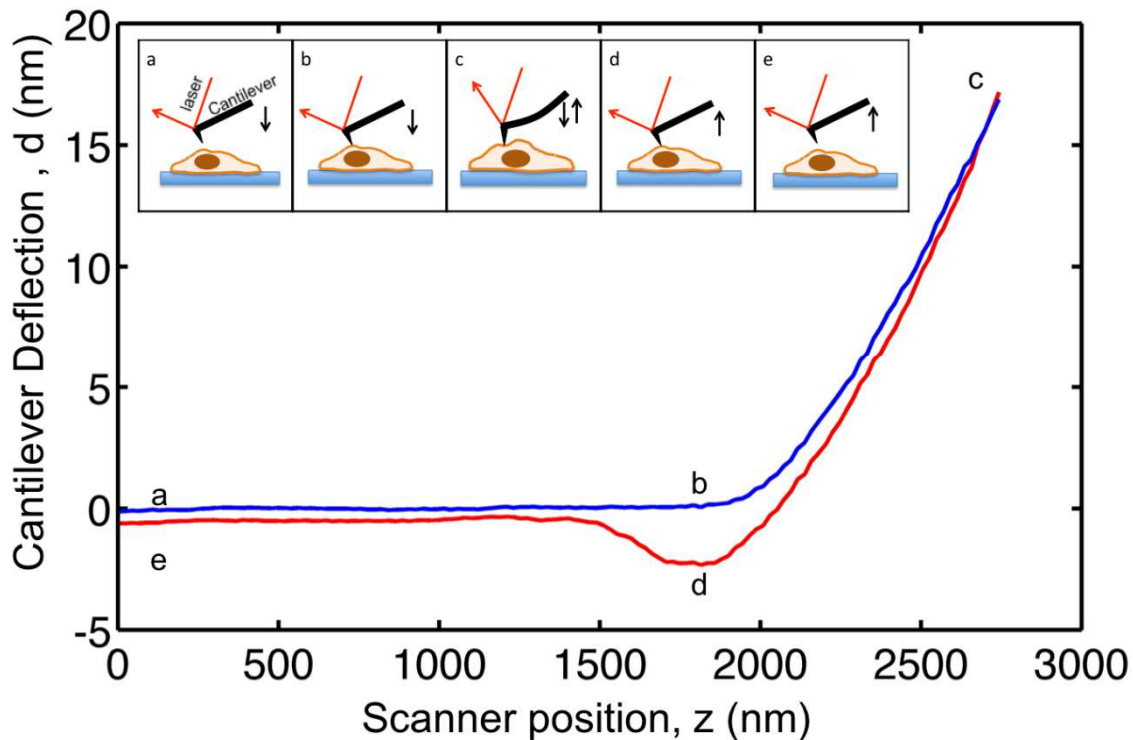
Figure 7. Illustration of AFM microindentation and interpretation of the force curve. The AFM starts from point a, a few micrometers above the cell. While approaching the cell, the AFM cantilever deflection remains zero until it reaches point b, where the tip comes into contact with the cell. The coordinates of point b are critical values for data analysis, denoted by $(z0, d0)$. From b to c, the cantilever indents into the cell until the cantilever deflection reaches a set point, which is set to be the ratio between the targeted maximum indenting force and the cantilever spring constant. In this plot here, the maximum indentation of a cantilever, of which the spring constant is measured to be 0.07N/m, is set to be 17 nm so that the maximum indenting force applied to sample is 1.2 nN. Once the deflection signal reaches the preset maximum value, the cantilever is then withdrawn from the cell to point d, where it often be pulled downwards due to tip-sample adhesion, detaches from the cell and returns to its initial location at e.

Calibration

The deflection of an AFM cantilever is measured by reflecting a laser beam from the end of the cantilever. The reflected beam is incident on a position-sensitive detector (PSD) whose output is measured in volts. To make this information useful, it must be converted into a distance (the actual displacement of the cantilever tip from its equilibrium position), which can then be used to calculate the force applied to the sample. This is accomplished through two calibration procedures to determine the cantilever sensitivity, in m/V, and the cantilever spring constant, in N/m. Within the range of motion detectable by the photodiode, both of these calibration factors are taken as constant.

The cantilever sensitivity is determined by pressing the AFM tip against a stiff surface, such as glass or mica, and measuring the resulting photodiode voltage as a function of vertical piezo displacement. Under the assumption that the calibration surface does not deform significantly, the cantilever deflection should be equal to the vertical piezo travel. Therefore, the cantilever sensitivity can be backed out from the slope of the curve,

$$\sigma \frac{dV}{dz} = 1,$$

where V is the photodiode reading, and z is the piezo position. This slope can be determined to high accuracy by performing a least-squares linear fit to the post-contact portion of the voltage-distance curve. The value σ is often termed the "optical lever sensitivity" due to its dependence on the reflected laser beam. If the position of the laser spot on the cantilever changes after calibration, the sensitivity will change, and must be re-calibrated. Additionally, this sensitivity is dependent upon the refractive index of the medium surrounding the cantilever, and therefore must be calibrated in the same medium (e.g. water, air) as used for experiments.

The spring constant may be calibrated by a number of different methods. The simplest approach is to measure the dimensions of the cantilever beam (often provided by the manufacturer) and use the known elastic modulus of the material – typically Si or SiN – to compute the stiffness using beam theory. For example, the spring constant of a rectangular beam is given by

$$k = \frac{Ewh^3}{4L^3}$$

where E is the elastic modulus, and L, w and h are the beam's length, width, and thickness, respectively. Similarly a triangular cantilever is equivalent to two such rectangular beams in parallel. This method has significant disadvantages; in particular, it is highly sensitive to the cantilever thickness which is difficult to measure accurately. Additionally, it is sensitive to nonuniformities in the elastic modulus which may be caused by material impurities, or the reflective gold coating often used on SiN cantilevers.

A better approach, known as the thermal or equipartition method, relies on measuring the thermal power spectrum of the suspended cantilever. This can be done using the AFM detection system, provided that the cantilever sensitivity is already known. From the equipartition theorem, a 1D harmonic oscillator subject only to thermal excitations will behave as

$$\frac{1}{2}k\langle x^2 \rangle = \frac{1}{2}k_B T$$

where k is the oscillator spring constant, x is the displacement from equilibrium, k_B is Boltzmann's constant, and T is the temperature. Finding the spring constant should therefore be a simple matter of measuring the displacement and temperature and computing a time average.

This matter is complicated somewhat by the fact that a cantilever beam is not actually a simple harmonic oscillator, but in fact has multiple bending modes, and therefore multiple modes of oscillation. When measuring the thermal motion of such a system, multiple peaks appear at different resonant frequencies, which each correspond to a different mode and a different "spring constant" associated with that mode. For quasi-static force measurements, the only mode of interest is the first, fundamental bending mode of the cantilever, so the higher order peaks should be excluded from the power spectrum data before calculating the spring constant. Once the fundamental peak is isolated, it can be fitted to a function of the form [55]

$$\frac{P(f)}{\Delta f} = \frac{\alpha}{\left[1 - \left(\frac{f}{f_0}\right)^2\right]^2 + \left[\frac{f}{f_0 Q}\right]^2},$$

where α is a normalization constant, Δf is the frequency resolution, f_0 is the natural frequency, and Q is the quality factor equal to $\sqrt{km}/b$, where b is the damping coefficient. The normalization constant α turns out to be $4/(\omega Q)$, where ω is the kinetic resonant frequency of the cantilever, $\sqrt{k/m}$. Following the calculation employed in Ref. [55], the squared displacement of the cantilever follows the density distribution

$$\frac{x^2(f)}{\Delta f} = \frac{4k_B T}{\omega Q k} \frac{1}{\left[1 - \left(\frac{f}{f_0}\right)^2\right]^2 + \left[\frac{f}{f_0 Q}\right]^2}.$$

Finally, the spring constant can then be determined from the parameters f_0, Q, Δf, and the squared peak amplitude, $x^2(f_0)$.

$$k = \frac{2k_B T Q}{\pi x^2(f_0)} \frac{\Delta f}{f_0}.$$

Indentation of adherent cells

Once the spring constant and the optical lever sensitivity are calibrated, the instrument is ready to be used for quantitative force measurements. Nearly all commercial AFM systems are equipped with a "force spectroscopy" mode, in which the cantilever is lowered at a constant velocity until a user-specified "trigger" force is reached, and then retracted. To perform force spectroscopy measurements of cells, a healthy cell is first selected with the aid of an optical microscope and positioned beneath the tip of the AFM cantilever.

To obtain accurate measurements, the force spectroscopy parameters and tip position must be carefully selected. Cells are inherently heterogeneous, so indentations performed above the nucleus may yield substantially different results than, for example, the cytoskeleton. For this reason, it is important to carefully position the targeted portion of the cell below the cantilever tip. Additionally, the trigger point must be carefully selected in order to avoid rupturing or otherwise damaging the cell due to excessive force. Finally, the tip velocity and retraction distance can also affect measurements due to viscous and hydrodynamic effects. Table 1 gives an overview of typical parameters used to measure cells.

Parameter	Recommended Range of Values
Trigger Force	200-800 pN
Approach / Retraction Distance	10-15 μm
Tip Velocity	1-2 μm/s

Table 1. Typical values of force curve parameters.

Due to the heterogeneous nature of the cytoskeleton, a single force curve cannot be assumed to represent the average or typical stiffness of the cell. To obtain an accurate sense of cell stiffness, it is necessary to perform at least 3-4 force curves at different locations on the cell and average them. Many commercial AFMs include a "force mapping" function, which automatically

performs force spectroscopy measurements in a raster grid over a pre-determined area. This can be a powerful method to map the change in stiffness over different regions of a cell.

While it is important to collect sufficient data for reliable statistics, care must be taken not to over-indent any particular cell to avoid causing changes in cell stiffness resulting from cytoskeletal rearrangement or cell-generated responses to indentation. Therefore, the recommended procedure is to collect only 3 curves per cell, while sampling as many cells as is feasible in any particular experimental group.

Data analysis

We analyze the recorded force curves using a custom MATLAB procedure to calculate the cell stiffness. First, the point of initial contact is identified by iteratively performing a fit of the Hertzian model (discussed below) to find the starting point at which the total RMS fitting error is minimized. Then the sample deformation δ and indenting force F are calculated as:

$$\delta = \begin{cases} 0 & z < z_0 \\ (z-z_0)-(d-d_0) & z \geq z_0 \end{cases}, \text{ and } F = \begin{cases} 0 & z < z_0 \\ k(d-d_0) & z \geq z_0 \end{cases}$$

where (z_0, d_0) is the point of contact.

Finally, a least squares fitting is applied to fit the F vs. δ data in the post-contact region, $z \geq z_0$, to the Hertz model to extract the Young's modulus, E of the cell:

$$F = \begin{cases} \dfrac{4ER^{0.5}}{3(1-v^2)}\delta^{1.5} & \text{Spherical tip of radius } R \\ \\ \dfrac{2E\tan\varphi}{\pi(1-v^2)}\delta^2 & \text{Sharp cone tip of opening angle } 2\varphi \end{cases}$$

where v is the Poisson's ratio, usually taken to be 0.5. For bulk cell stiffness measurements, it is usually advisable to use a spherical tip to reduce the maximum strain on the membrane. However, conical tips are useful for probing fine features of the cell such as cytoskeletal filaments or neuronal axons.

18

Results

Figure 8a shows three representative force curves taken from 3T3 fibroblasts cultured on plastic surface, polyacrylamide gel of Young's moduli 3000 Pa and 17000 Pa, respectively. After carefully identifying the contact points in the curves, we calculate the indenting force as function of cell deformation. As shown in **Figure 8**b, under a force of magnitude smaller than 0.3 nN, a pyramid shape tip indents 3 micrometers into a cell cultured on a 3000 Pa polyacrylamide gel. To indent 500 nanometers into the cell grown on plain culture dish using the same tip, a force more than 1.6 nN is required. It is clear from this graph that the cell cultured on soft polyacrylamide gel is softer than the cell cultured on the stiff culturing dish. Fitting the force-δ curves to the Hertz model gives Young's moduli of the three cells as 10 kPa, 1.2 kPa, and 0.1 kPa, respectively. Cells on the culture dish are 100 times stiffer than cells cultured on polyacrylamide gels. Solon et al have reported similar results [52]. They found that fibroblasts actively stiffen their cytoskeletons to match the stiffness of substrates they adhere to. Many other cell types have also been reported to become stiffer when cultured on stiffer substrates [56].

Figure 9a shows a fluorescence image from a 3T3 fibroblast on a cell culture dish. The cell is transfected with GFP vimentin, a type of intermediate filaments. AFM Force-mapping has been performed in this 80 μm by 80 μm area, with a resolution of 32x32 pixels. The resulting stiffness map is shown in **Figure 9**b. The stiffness varies across the cell, with the lamellipodium region showing larger and more heterogeneous values of the Young's modulus than the perinuclear region, which surrounds the stiff nucleus.

The cell thickness varies from <1 μm in the lamellipodium region to ~10 μm at the nucleus. Because of this, the stiffness measured at the extreme edges of the cell may be influenced by the substrate. To minimize this effect, only the first 100nm of loading data were used for the Hertz model fit.
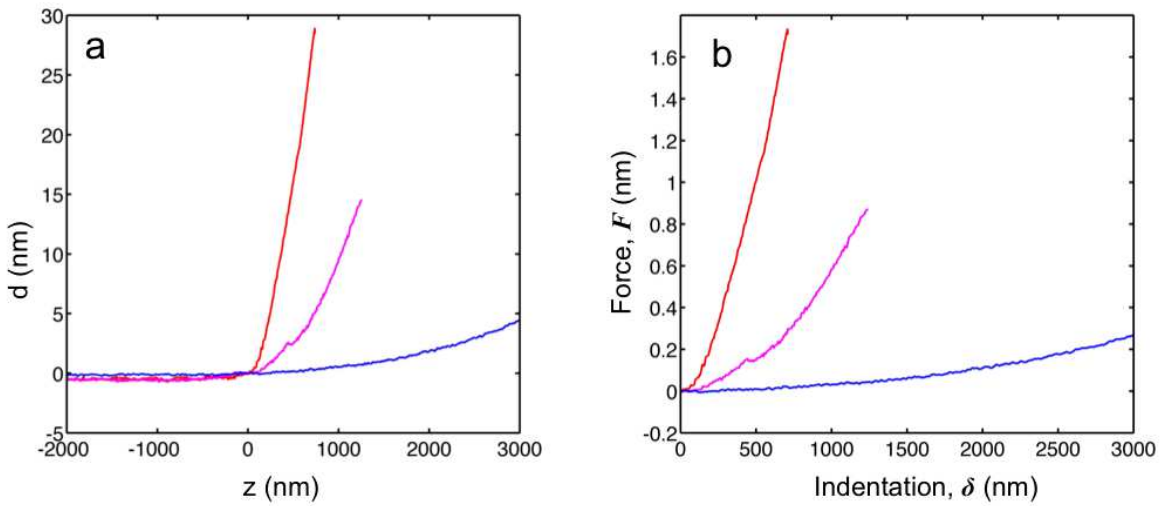
Figure 8. Force curve data and the analyzed force-indentation curve. a) A set of three representative force curve data acquired for 3T3 fibroblasts cultured on glass (red), 17 kPa polyacrylamide gel (purple), and 3 kPa polyacrylamide gel (blue). b) The force-indentation curves calculated from a). The spring constant of cantilever is 0.062 N/m in this case.
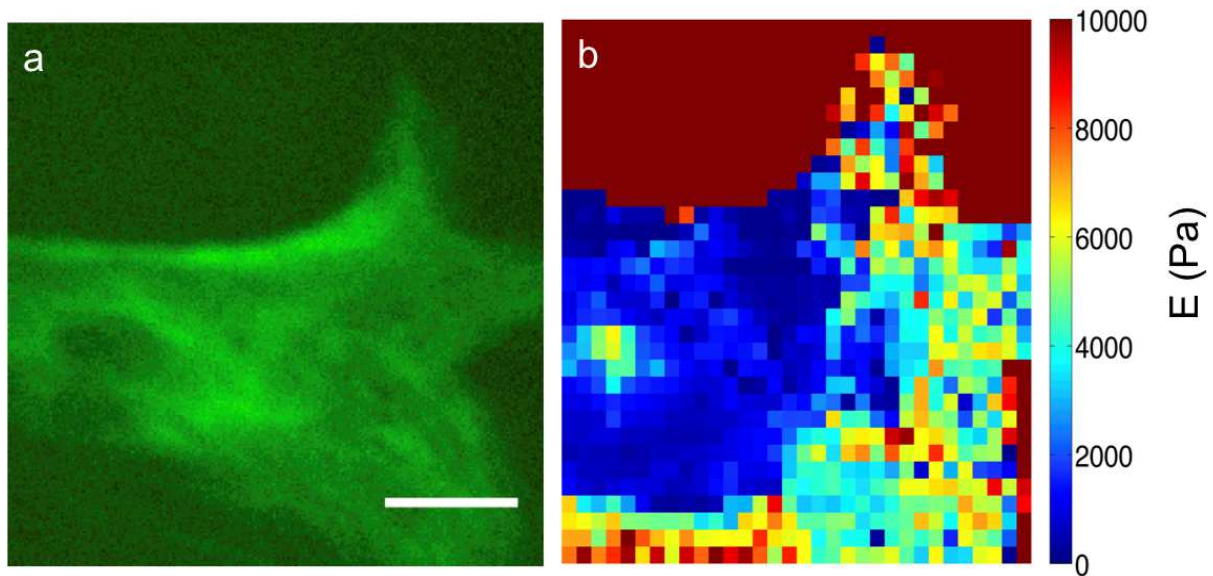
Figure 9. Stiffness mapping of cells. a) Fluorescence image of a 3T3 fibroblast transfected with GFP vimentin. Only a part of the cell is shown in the image. Scale bar represents 20 μm. b) A 32x32 pixel stiffness map of the same area. Each pixel represents 2.5 μm.

Discussion

Advantages of the AFM method

The AFM indentation method has advantages to characterize mechanical properties of living cells. The sensitivity to changes in forces makes it possible to detect weak resistance force from soft samples on the pN level. The high spatial resolution makes it possible to characterize on the submicron level the heterogeneities in tissues and within single cells [57]. It also allows real-time live cell measurements. Several AFM models designed for biological samples can operate in a fluid environment and are equipped with heated sample stages, which provide precise temperature control, making it possible to maintain a physiological environment for living cells during the measurements. AFM indentation has been successfully applied for measuring the mechanical properties of a range of cell types [52, 58-60], and has been used extensively for assessing changes in mechanical properties of cells associated with cellular differentiation and in various disease contexts [56, 61].

An important step in data analysis is identifying the point where the tip first makes contact with the cell. This has great impacts on the analysis of cell stiffness, as a variation of ±25 nm in the contact point can affect the elastic modulus by up to 10% [62]. For stiff materials, the deflection signal increases abruptly after the tip-sample contact, and the contact point is readily identified as turning point in the curves. Such a sharp turning point, however, often does not appear in the force-curves from cells, due to the low cell stiffness (see **Figure 8**a). The uncertainty in contact point gives large uncertainty in cell stiffness since calculations of sample indentation and indenting force are strongly dependent on the location of contact point. We developed a MATLAB code to accurately find the contact points in force curves from soft samples using the algorithm proposed by Lin et al. [63]. The code is able to accurately process most of the force curves from soft samples. This code enables us to automate the process of data analysis by automatically searching for the contact point and fitting the indentation data to Hertz model.

The stiffness range that can be reliably measured spans from less than 100 Pa to 10^6 Pa, covering the stiffness range for most of the tissues and cells. To make reliable measurements, it is important to select the AFM cantilevers with spring constants well matched to the sample stiffness. When the probe is too stiff, its deflection is too small to detect and it could damage the cell; if the probe is too compliant, it will not indent the cell sufficiently to obtain reliable material

properties and its thermal vibrations can dominate the force curve. Cantilevers of 0.06 N/m with a pyramid tip are applicable for most cell types cultured on stiff culture dishes. These cantilevers, however, are not applicable to measure cells cultured on soft substrates. As shown in **Figure 8**b, the cell cultured on a 3000 Pa polyacrylamide gel is so compliant that only a 0.3 nN force is required to create a 3 μm indentation. The force curve is so flat that there is very little difference between the pre-contact and post-contact region. This leads to large uncertainty in the contact point and hence the resulting stiffness values. In this situation, it is better to use a cantilever with large spherical tip. A 0.06 N/m cantilever with a spherical tip of 10 micrometers in diameter can be applied to measure samples with stiffness lower than 100 Pa. Cantilevers with spherical tip are commercially available from many vendors. They can also be custom-made by gluing microspheres to tipless cantilevers. The spherical tips provide larger deflection signal and prevent damage to the cell membrane. However, they are not applicable for high-resolution stiffness mapping, due to their large contact area with the cells. Table 2 provides a list of AFM probes with applicable stiffness.

Model	Spring constant (N/m)	Tip Type	Tip radius (nm)
Bruker DNP10-D	0.06	Pyramid	20
Bruker MLCT-B/C/E	0.01/0.02/0.03	Pyramid	20
Novascan PT.GS	0.3	Sphere	5000
Nanosensors PL2-CONT	0.2	Punch	900

Table 2. A selection of AFM probes with applicable stiffness and tip geometry for cell indentation.

Limitations

The Hertz contact mechanics model we commonly use to fit the indentation data is a simplistic model. It predicts the force-indentation relationship for infinitesimal indentations of purely elastic materials by axisymmetric indenters. Some of the assumptions of the Hertz model do not apply to the cell indentation.

The Hertz model assumes homogeneous and linearly elastic material, while a cell is heterogeneous (see **Figure 9**) and nonlinearly elastic. In the lamellipodium region, it is rather inhomogeneous due to the heterogeneous structure of the actin cytoskeleton. To report the

mechanical stiffness of a cell, we take the average of three or more curves acquired from the relatively homogeneous perinuclear region [52, 60]. Reconstituted networks of actin and intermediate filament are strain-stiffening materials, i.e. they are stiffer at larger deformations [64, 65]. Such a nonlinear elasticity has been observed for living cells, but not accounted for in the Hertz model. To limit the effect of nonlinear elasticity on the reported cell stiffness, we only fit the first 250 nm of the indentation data to the Hertz model.

It is also assumed in the Hertz model that the materials are purely elastic. However, cells and their cytoskeleton are viscoelastic materials with stiffness dependent on the time scale of measurements. At shorter time scale, the cantilever deflection mainly comes from the elastic response of cells. At long time scale, however, the sample creeps and gives a softer response. The time scale of AFM indentation is controlled by tip velocity. Hence, the observed difference in cell stiffness is only meaningful when the force curves are acquired with the same indentation velocity. To quantitatively extract the frequency dependent viscoelasticity of cells, the AFM "force modulation" method has been developed by applying high frequency small amplitude oscillations upon a larger indentation [48, 54].

Stilwell and Tabor [66] showed that the unloading segment, rather than the loading segment of the curve can be accurately related to Young's modulus without the need to account for viscoelastic or plastic deformation of the sample. However, using the retraction curve from an adhesive material such as a cell can lead to a wrong calculation of the contact area due to adhesion between the tip and sample [67, 68].

Future Work

The assumption of infinite sample thickness in the Hertz model does not apply for cells. Cells are typically a few micrometers thick in the perinuclear region, and a few hundred nanometers thick in the lamella region. Corrections have been made to account for the finite sample thickness [65, 69]. Data acquired from force-mapping contains both indentation data and cell height, so the local sample thickness can be calculated from the height. Future work is required to implement the sample thickness corrections in our analysis for force-mapping data.

In addition to the assumption of infinite thickness, the Hertz model is simplistic in its requirement for a specific indenter shape function (sphere or cone) and assumption that the indentation during loading and unloading are the same for an applied force. A method introduced

by Oliver and Pharr [70] provides an improved way to determine the elastic modulus and hardness of a material, which can be used for any indenter shape and is not affected by plastic deformations of the sample. The elastic force is measured using the beginning of the unloading segment of the curve, where the measured force is purely a restoring force from the deformed sample. The subsequent calculation of hardness is based on the premise that for any indenter, the load is related to the indentation by a power law

$$P = A(d - d_{max})^m$$

where P is the load, $d - d_{max}$ is the elastic deformation, and A and m are fitting parameters both related to the material properties. This differs from the Hertz model in that the latter employs a fixed value of m based on the assumed tip geometry, rather than determining the value from a least-squares fit. Future implementations of our stiffness measurement method should include this improvement when calculating either the elastic modulus or hardness of the cells.

Chapter 4 – Characterizing the integrin-ligand bonds

Having observed the cells' mechanical response to changes in substrate stiffness, our focus of investigation shifted toward the mechanical pathways that may allow cells to sense these changes and generate a response. As discussed in Chapter 2, the integrin-ligand interaction is thought to act as a mechanical sensor, making use of conformational changes in integrin structure and binding site accessibility based on applied tension. This knowledge generated motivation to investigate whether the integrin-ligand bond structure or kinetics can change on different substrates.

Measuring adhesive forces

The AFM's ability to resolve sub-pN vertical forces makes it an ideal tool for studying molecular-level adhesions. In addition to applying a compressive force, the AFM can also be used in reverse force-spectroscopy mode to apply pulling forces of several nN. This requires that the AFM cantilever be strongly bound to the measured sample, in such a way as to ensure that the adhesive link being studied is the weakest component of the cantilever-sample-substrate system. In the simplest type of experiment, adhesion measurements can be obtained without any special treatment of the AFM cantilever (**Figure 10a**). The force data recorded during retraction of the cantilever while performing force spectroscopy gives information about the attractive interaction between the sample and the cantilever tip, and the usefulness of this information is limited based on the chemistry of the interaction between the sample and whatever the cantilever is made of, typically silicon or silicon nitride.

A more useful study involves functionalizing the AFM tip with a selected molecule or "probe" which is then brought into contact with the sample (**Figure 10b**). The measured force as a function of retraction distance gives insight into the interactions between the probe and sample. This method can be generalized by attaching any object (size permitting) onto the end of the AFM cantilever to be used as a probe for adhesion measurements (**Figure 10c**).

The first two methods can be applied easily to adherent cells. Numerous studies over the past two decades [71-73] have established a collection of accepted bond strengths for protein-cell and protein-protein interactions. This setup is not ideal, however, for studying cell-ECM interactions: Regardless of the coating on the AFM tip, the cantilever and tip themselves play a large role in

the interaction. The mechanical properties of silicon (or silicon nitride) are not at all similar to tissue, cells, or extracellular matrix, and therefore do not mimic the in-vivo interaction mechanics closely enough to provide meaningful results [74].

An accepted method of measuring cell-ECM interactions is to mimic the ECM with a protein-coated polyacrylamide gel substrate (with tunable stiffness), and then attach a suspended cell to the AFM cantilever by a layer of protein such as Concanavalin-A [74]. This essentially inverts the experiment, with the cell now being used as a probe, and the ECM ligands bound to the soft substrate. (c). We used this method to investigate whether the integrin-ligand bond strength is regulated by ECM stiffness.
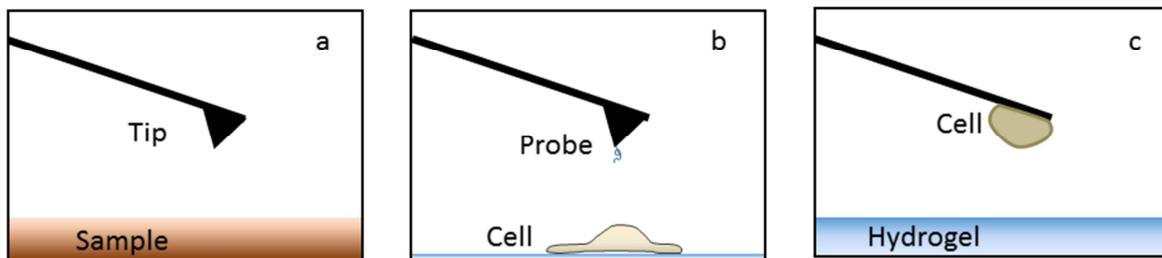
Figure 10. Illustration of different adhesion measurement experiments. a) Untreated AFM tip and a sample. b) probe-functionalized AFM tip and a sample. c) Adhesion measured between two samples: one attached to the cantilever, and one attached to the stage.

Substrate Preparation

Polyacrylamide gels were prepared according to the method described by Pelham & Wang [75]. Gel stiffness is controlled by varying the concentrations of acrylamide and bisacrylamide (Biorad) as shown in Table 3. The heterobifunctional crosslinker Sulfo-SANPAH is used to covalently link collagen to the gel surfaces. A solution of collagen at various concentrations was first combined with 1 mg/ml Sulfo-SANPAH and incubated in the dark for 2 hours at pH 4.5. This solution was then added directly to the gel surface, and incubated under 365 nm UV irradiation for 10 minutes. Gels were then rinsed repeatedly with PBS buffer, then blocked with 0.1 mg/ml bovine serum albumin (BSA) for 30 minutes. The collagen-coated polyacrylamide substrate was then rinsed exhaustively and secured in a 50 mm polystyrene dish. Before introducing cells, the gel stiffness was characterized using AFM force spectroscopy [2].

A total of 4 polyacrylamide gel conditions in the range 3.5kPa – 65kPa were used. Within each stiffness condition, samples were prepared with a high collagen density (0.1 mg/ml) and a low collagen density (0.3 µg/ml) coating.

Acrylamide (%)	Bisacrylamide (%)	Elastic Modulus (kPa)
5	0.08	4 ± 1
8	0.10	18 ± 5
12	0.14	40 ± 10
16	0.20	60 ± 10

Table 3. Concentrations of acrylamide and bisacrylamide used to produce hydrogels of varying stiffness

Single-Cell Force Spectroscopy

AFM-SCFS experiments were performed on an MFP3D-BIO Atomic force microscope (Asylum Research, Santa Barbara, CA). The SCFS protocol was adopted from [73]. Briefly, an NIH-3T3 fibroblast was attached to an AFM cantilever, pressed against the polyacrylamide gel surface for a pre-set contact time, and then pulled away from the gel surface. The measurement procedure, including a representative force curve for cell-substrate unbinding, is illustrated in **Figure 11**. The detachment process is consists of small, discrete unbinding events, manifested as instantaneous jumps in the measured force during retraction.

To promote cell attachment, tipless AFM cantilevers (Bruker NP-O10) were coated with concanavalin-A (ConA). The cantilevers were first cleaned in oxygen plasma at a power of 100 Watts for 90 seconds and then immersed in a solution of 1 mg/ml Con-A (Sigma-Aldrich) for 30 minutes at room temperature. Cantilevers were then rinsed exhaustively with DI water and air dried. Prior to obtaining force measurements, each cantilever was calibrated to determine its spring constant [2].

NIH-3T3 fibroblasts were cultured in modified Dulbecco's Eagle's Medium (DMEM) supplemented with 10% bovine calf serum and 2mM L-Glutamine. Immediately prior to experiment, the cells were washed with PBS buffer and incubated in 0.05% trypsin+EDTA for 3 minutes, resuspended in DMEM, and centrifuged for 5 minutes at $200 \times g$. After removing

DMEM the cells were washed with PBS, centrifuged a second time, and finally suspended in PBS buffer supplemented with 1 mM $CaCl_2$ + 0.5mM $MgCl_2$. To attach a single cell to the AFM cantilever, the suspended cells were introduced to the prepared dish at low density such that a single cell could be isolated. Aided by optical microscopy, a healthy, unattached cell was located and positioned under the end of the AFM cantilever. The cantilever was engaged gently (~500 pN) onto the cell and then withdrawn. After verifying that cell-cantilever contact was maintained, the cell was allowed to rest for 5 minutes to fully attach to the cantilever.

Measurements by Zhang et al. [76] have determined that the force required to disrupt the cell-cantilever attachment using Con-A is > 2nN. Given that integrin-ligand unbinding forces have been measured on the order of ~100 pN [37, 38, 72-74, 77-80], we have reasonable assurance that the breaking events are most likely to occur at the cell-substrate interface rather than at the cell-cantilever interface.

With the cell firmly attached to the AFM cantilever, force spectroscopy measurements were performed against the polyacrylamide substrate. The cell was pressed against the substrate with a force of 500 pN for a controlled contact time, and then retracted at a velocity of 2 μm/s. Measurements were taken using both long (60 s) and minimal (100 ms) contact times. A total of at least 128 curves were collected for each sample condition, using a minimum of 3 cells. Each curve was acquired at a different location on the gel using the Force Mapping function.
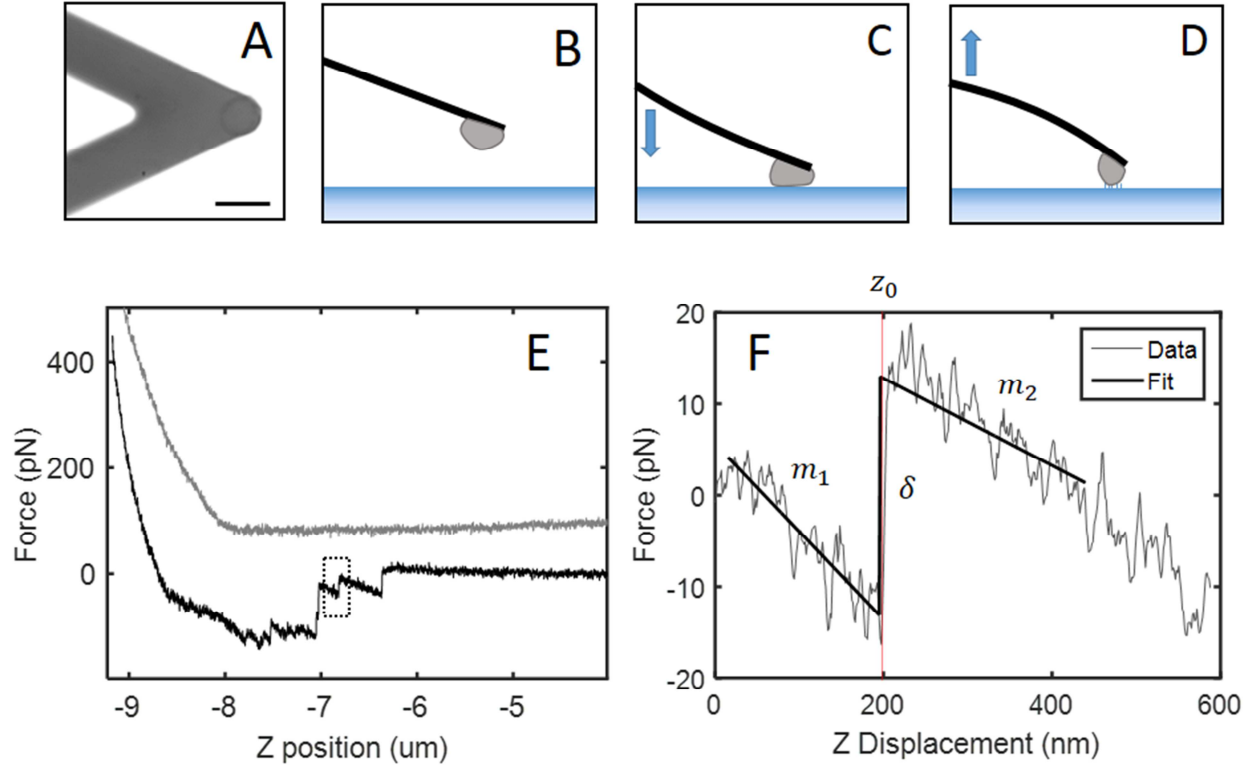
Figure 11. Illustration of the AFM-SCFS measurement procedure. (A) Bottom-view image showing a cell attached at the end of the AFM cantilever. (Scale bar: 25 μm). (B)-(D) The process of force-curve collection. The cantilever with a cell (B) is driven by the AFM to approach the gel surface (C) until a contact force of 500 pN is reached. After contacting the gel for 60 seconds, the cell is then pulled away (D) until it is totally separated from the surface (B). The resulting force curve of this process is shown in (E). The gray curve represents the process of bringing the cell to the surface (approach), and the black curve represents the process of pulling the cell away from the gel surface (retraction). The jumps in the retraction curve correspond to the rupture of the integrin-ligand bonds. Each rupture event is selected (boxed region) and fitted to a step function as shown in (F). F shows a jump with the fitted Heaviside function overlaid. m_1 is the loading rate prior to detachment, and δ is the jump magnitude.

Data analysis

Bond dissociation events in the obtained AFM curves were detected using a custom MATLAB procedure based on the work of Opfer and Gottschalk [81]. Briefly: the retraction portion of the curve was first flattened by a moving-average filter to remove low-frequency information, leaving only the high-frequency jump events. This resulting curve was then transformed using an iterative stationary Haar wavelet transform. After selecting a threshold value based on the signal's RMS noise level and the minimum expected step size, the transformed signal was thresholded and inverse-transformed. Finally, the thresholded signal was differentiated, and a peak-finding algorithm was used to identify local maxima. These peaks in the differentiated

signal correspond to step discontinuities in the original, unfiltered signal. Examples of the original, thresholded, and differentiated signals are shown in **Figure 12**.
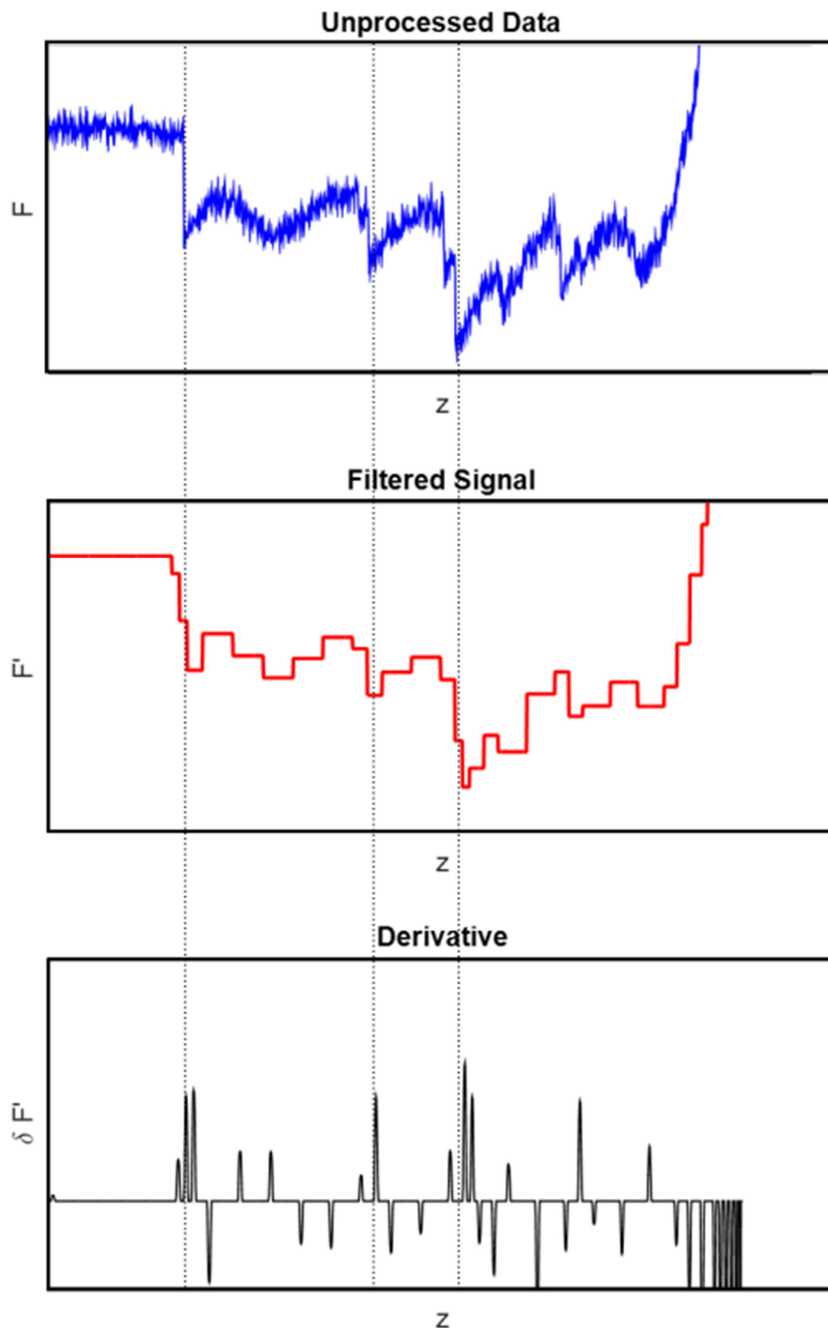
Figure 12. Stages of retraction curve processing. Top: The original, unfiltered retraction segment including discrete unbinding events. Middle: The same signal after filtering by the Haar-wavelet transform. Bottom: pointwise differential of the thresholded signal. The dashed lines illustrate the correspondence between peaks in the differentiated signal and steps in the original signal.

The primary motivation for using an automated jump detection algorithm was due to the large amount of data collected. For each experimental group, we collected between 200 and 500 force-distance curves, and analyzing each curve by hand quickly proved to be prohibitively time-consuming. Nevertheless, the automated detection introduced a number of complications, which need to be considered before the results can be considered trustworthy.

As with any detection system, this algorithm suffers from two potential modes of failure: spurious events (detected events that do not correspond to true events) and missed events. We observed both of these modes with varying frequency, depending on the filtering threshold and noise level of the data. As discussed by Opfer, the selection of a threshold value following the wavelet decomposition is non-trivial and also critical to the performance of the detection algorithm. For our case, we decided to tune our detection preferentially toward a higher fraction of missed events than spurious events, to ensure that the remaining data would be trustworthy. For each data set, our threshold value was manually fine-tuned until the automated detection algorithm returned at least 85% of the same steps as were selected by hand from 5 curves chosen at random.

To obtain the force and loading rate to rupture a cell-ECM adhesion, the segment of the original curve surrounding each detected jump was fitted to a modified Heaviside function

$$F(z) = \begin{cases} m_1(z - z_0) & z \leq z_0 \\ m_2(z - z_0) + \delta & z > z_0 \end{cases}$$

where m_1 and m_2 represent the slopes of the curve before and after the jump, respectively, with dimensions of force/distance. z_0 represents the z-position at which the jump occurred, and δ represents the jump magnitude. The magnitude of the dissociation force is calculated from

$$F_d = \delta$$

and the loading rate is given by

$$r = m_1 v$$

where v is the user-selected AFM retraction speed.

Results

Loading rate and dissociation force depend on pulling speed

Since the substrate-cell-cantilever ensemble is modeled as a system of springs in series, it follows that that the loading rate applied to individual receptor-ligand bonds should be linearly dependent on the pulling speed. To confirm this, the SCFS measurements were performed using a collagen-coated glass coverslip as a substrate while varying the AFM retraction velocity from 0.5 to 10 μm/s. The result is shown in **Figure 13**. The measured loading rate and bond dissociation force each increase with the pulling speed. The loading rate shows an approximately linear relationship with the pulling speed, as expected, with an effective spring constant (representing the stiffness of the cantilever, cell, and substrate combined) of 0.006 N/m. The bond dissociation force increased logarithmically, in agreement with Bell's theory.
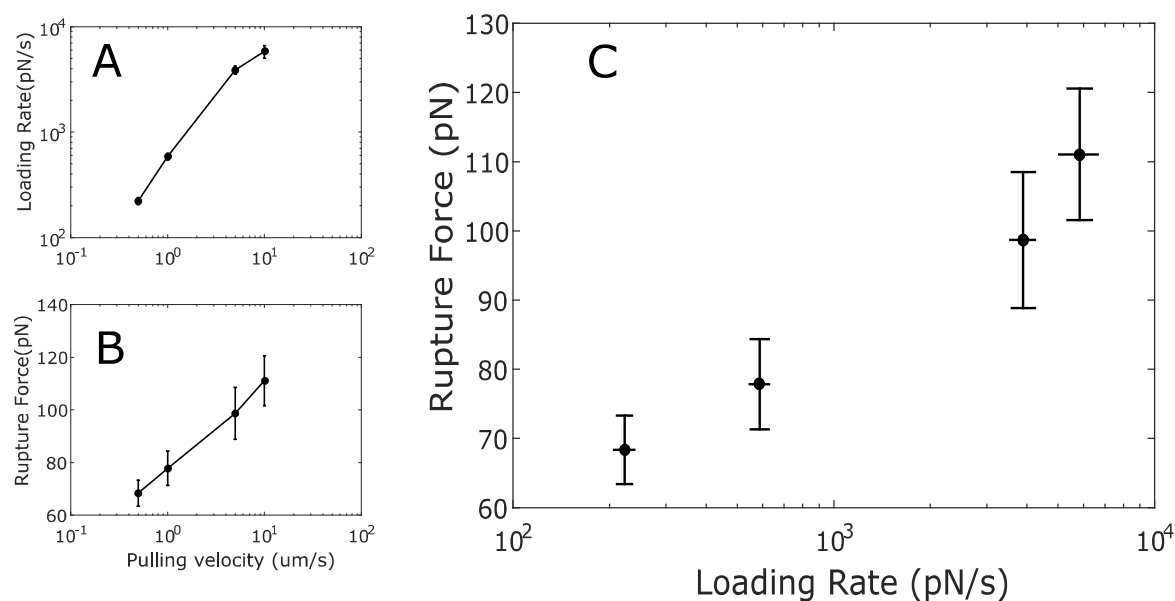
Figure 13. Measured loading rates and bond rupture forces on collagen-coated glass. (A) The loading rate increases approximately linearly with pulling speed, indicating that the substrate-cell-cantilever system behaves as a series of springs. (B). The bond rupture force increases logarithmically with pulling speed, and (C) the bond rupture force increases logarithmically with the loading rate.

Loading rate is not significantly affected by ECM stiffness

The series-spring model of cell-ECM interaction implies that changes in the stiffness of the substrate will lead to a change in the average rate of loading applied to receptor-ligand bonds, and subsequently a change in binding affinity. However, little evidence exists to suggest whether

32

or not the range of biologically relevant stiffnesses is large enough to elicit a substantial difference in the loading rate. Using a constant AFM retraction speed of 2 μm/s, we measured the loading rate of individual receptor-ligand bonds using SCFS on four collagen-coated polyacrylamide gel samples, ranging in stiffness from 3.5 kPa to 65 kPa. **Figure 14** shows the distribution of loading rates on each of the gels. The four gels produced a wide range of loading rates spanning more than three orders of magnitude (~1 pN/s to ~4000 pN/s), with median values of 140, 238, 159, and 96 pN/s, respectively. The difference in the loading rate between all samples was found to be insignificant ($p > 0.1$). Using a Monte-Carlo simulation to test a wider range of gel stiffnesses, we confirmed that this result is consistent with Bell's model (Appendix A: Monte-Carlo Simulation).
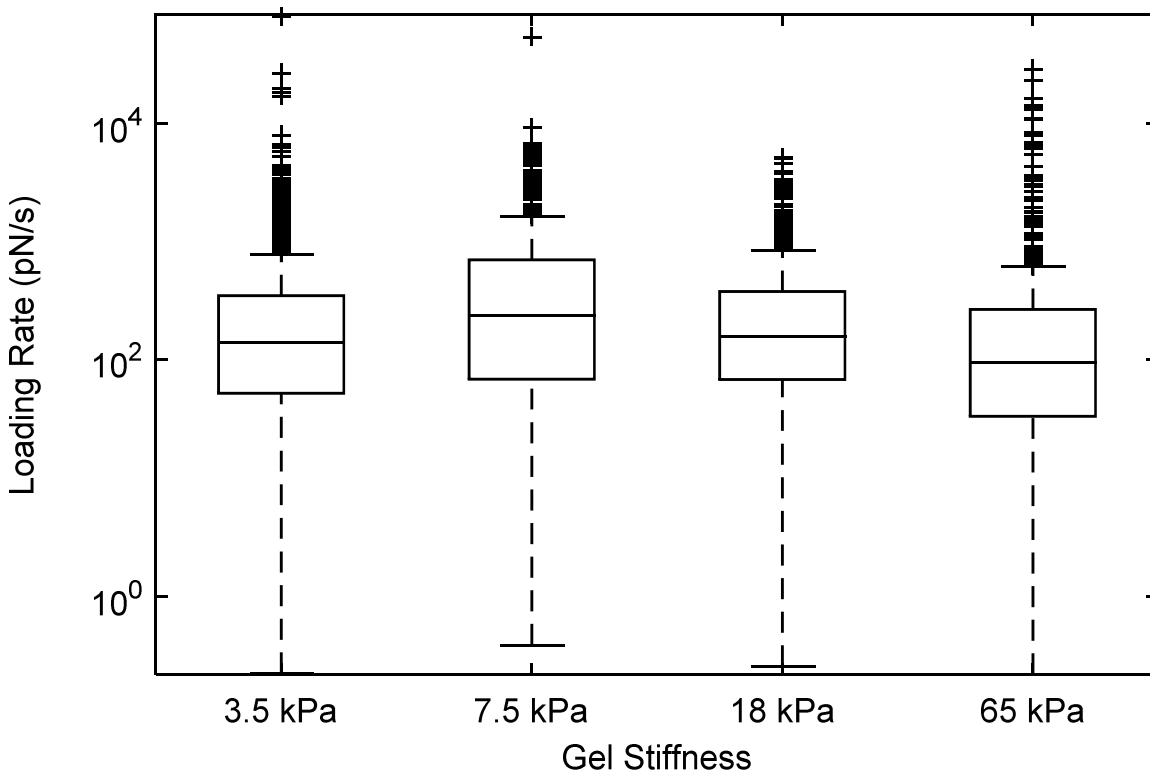
Figure 14. Loading rates measured on polyacrylamide gels of 3.5, 7.5, 18, and 65 kPa for rupture forces less than 200 pN. N = 767, 641, 827, and 789 events, respectively.

Rupture force of individual receptor-ligand bonds depends on contact time

From the gel measurements, the rupture forces associated with individual bond dissociation events were recorded and plotted as histograms as shown in **Figure 15**. Results showed a peak

dissociation force of 20 ± 5 pN with short contact times and 40 ± 20 pN with longer contact times. Although the peak values varied more widely between gels for the 60 s contact time than the 0.1 s contact time, the change was not statistically significant.
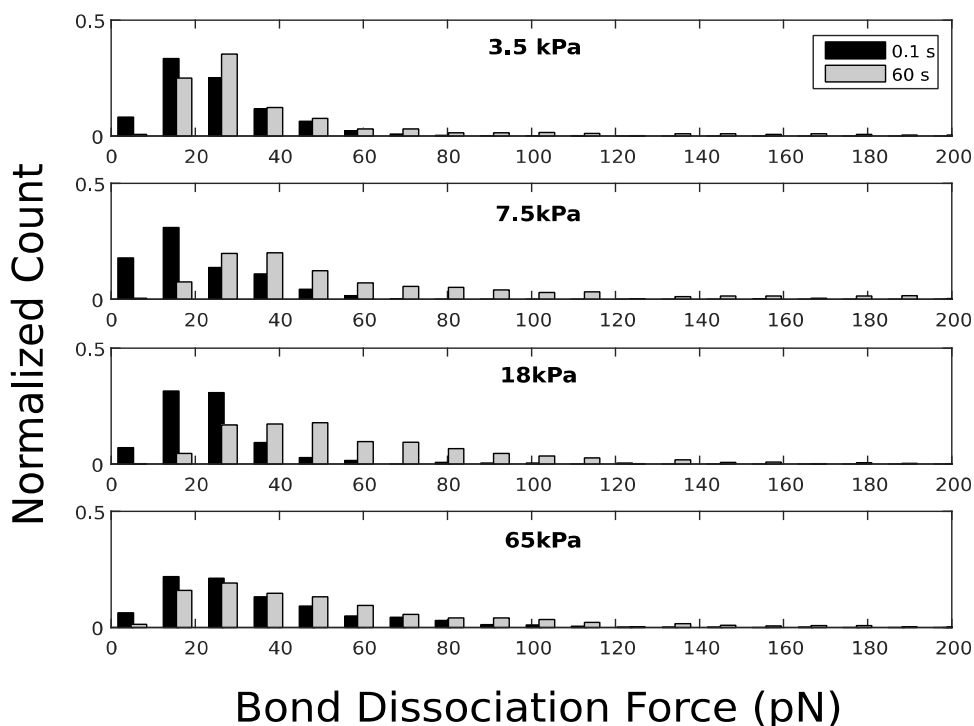
Figure 15. Histograms of individual receptor-ligand dissociation forces up to 200 pN. With 0.1 s contact times, the peak dissociation force is 20 ± 5 pN for all gels. With 60 s contact times, the peak is shifted into the range of 30-60 pN.

Low substrate stiffness promotes rapid integrin binding

As shown in **Figure 16**, the number of adhesion sites is initially larger on soft gels and decreases with stiffness. But after 1 minute of contact, the number of adhesion sites is roughly the same on all stiffness conditions. This agrees with a theory [82] that diffusion of ligands in the soft gels enables more rapid formation of nascent adhesions. This theory also suggests that although cells on stiff substrates require a longer attachment time, they should form denser integrin clusters and larger focal adhesions since the probability of integrin binding decreases sharply at locations away from previously existing bonds.

The number of adhesions increases with time for stiff substrates and decreases with contact time for soft substrates, contrary to the expectation that the number of adhesions on soft substrates should remain fairly constant with time. This observation indicates that during the initial seconds of contact, there may be some additional changes in integrin organization that we have not fully explained.
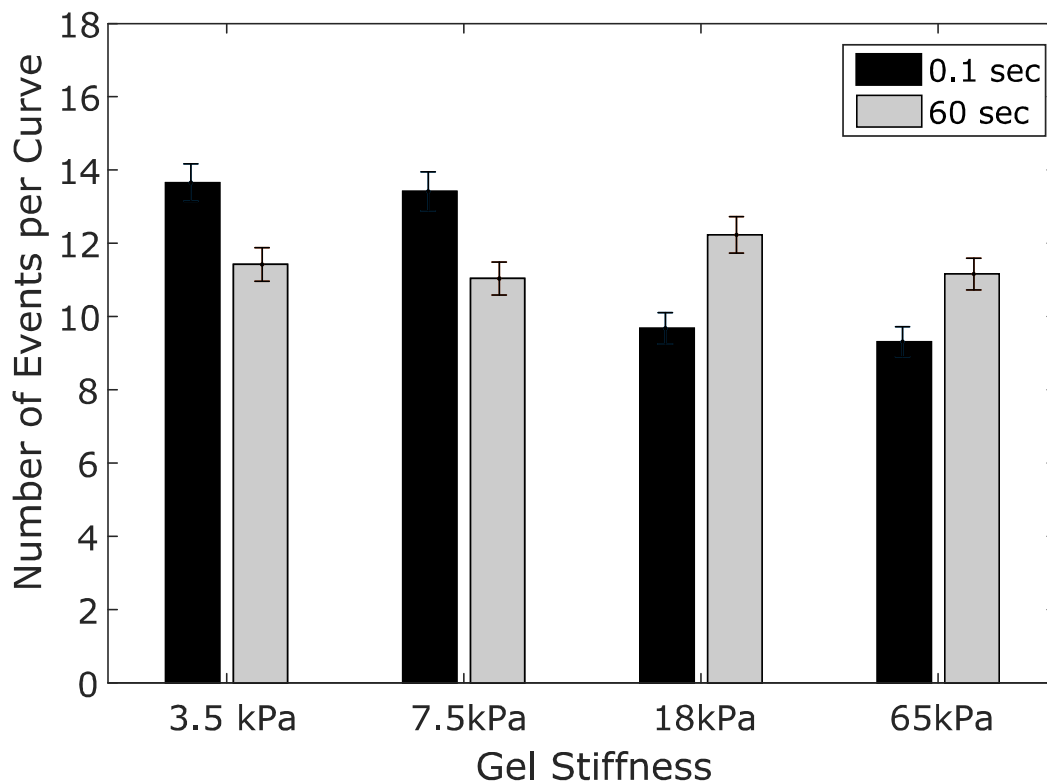
Figure 16. Number of dissociation events per curve indicating the number of adhesion sites. Within 100 ms of contact time, the softer gels promote formation of a large number of adhesions, whereas the number of adhesions on stiff gels is reduced. At longer contact times, the number of adhesions to the stiff gel matches the soft gel.

Integrin activation takes longer than 100 milliseconds

Previous AFM studies have reported rupture forces ranging from 40-200 pN for activated $\alpha 2 \beta 1$ integrins measured against stiff collagen-coated mica substrates[72, 73, 83]. For the dissociation force distributions in **Figure 15**, The peak force is determined to be 20 ± 5 pN for short contact times, and 40 ± 20 pN for longer contact times. This suggests that the unbinding forces observed following minimal contact time are not only representative of the activated integrins, but rather a combination of non-activated and partially activated integrins.

Numerous studies have established that integrins can exist in two major categories of conformational states: the active or "primed" state with high affinity for ligand binding, and the inactive state in which the active ligand binding site is inaccessible [84]. It is widely accepted that prior to attachment to the ECM, integrins in the cell membrane reside predominantly in the inactive state. Upon contact with a surface, the combination of nonspecific ligand binding and transmission of intracellular forces through the integrins can lead to activation of some integrins, subsequently allowing for the formation of catch bonds with high tensile strength.

To confirm that the increased bond strength at longer cell-ECM contact was due to integrin activation, we inhibited activation of the integrins by minimizing the presence of Mg^{2+} and Ca^{2+} ions using EDTA. Collagen-coated coverslips were incubated in standard PBS buffer supplemented with 2.5 mM EDTA for 30 minutes prior to experiment, and the same SCFS experiment was performed using 60 seconds of contact time. Under this condition, the individual bond rupture force was reduced to 30 ± 10 pN as shown in **Figure 17**.
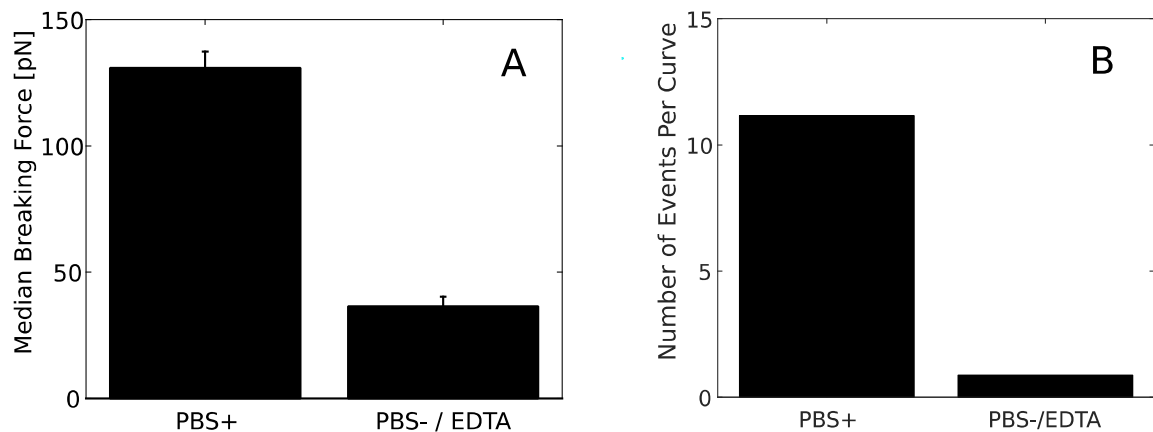
Figure 17. Individual bond dissociation forces with (+) and without (-) Ca^+ and Mg^{2+} on collagen-coated glass. The (-) condition also contained 2.5 mM EDTA to absorb extraneous ions. (A)Absence of these ions inhibits the activation of integrins, which reduces their binding strength. (B) Inhibition of integrin activation also reduces the total number of bound integrins.

Due to the large number of data points, it was not practical to display the results in a traditional scatter plot. A heat map showing the density of the events as a function of loading rate and bond dissociation force is given in **Figure 18**. After 60 seconds of contact, a significant number of bonds appear in the load-strengthening regime, as indicated.
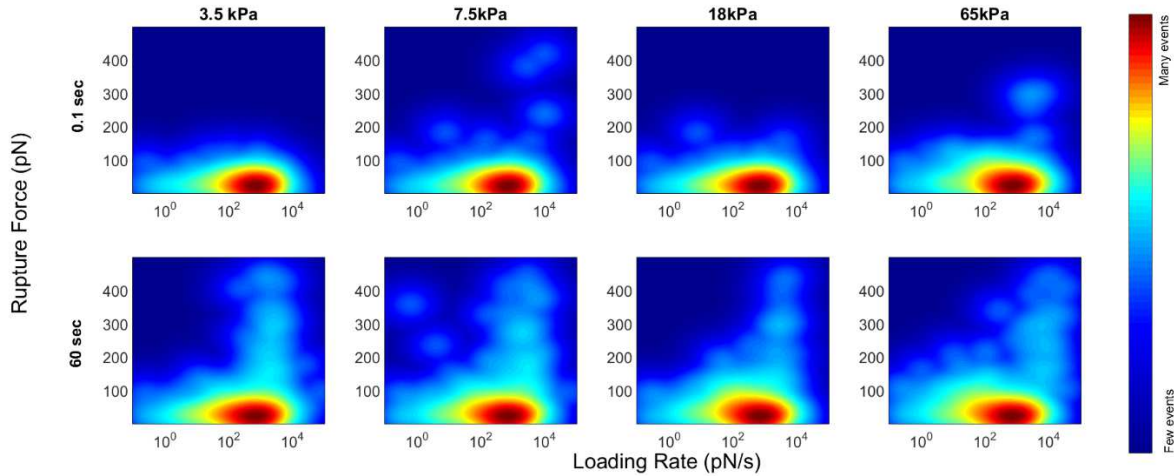
Figure 18. Heat maps showing the density of data points as a function of the loading rate and dissociation force for the 8 conditions measured. As indicated by the red arrow, the large rupture-force events that strengthen with the loading rate become pronounced after 60 seconds of contact.

Energy landscape of individual bonds is regulated by substrate stiffness

In **Figure 19**, the individual bond dissociation forces are binned and plotted as a function of their respective loading rates for both the 100 ms and 60 s contact times on the stiffest gel (65 kPa). The 60 s contact time shows a transition from the thermally-driven dissociation to the loading-dependent regime at loading rates of approximately 500 pN/s, as predicted by Evans and Ritchie [38]. However, this transition is not apparent with 100 ms contact time, suggesting that the integrin activation and specific binding occur on a timescale longer than 100ms.
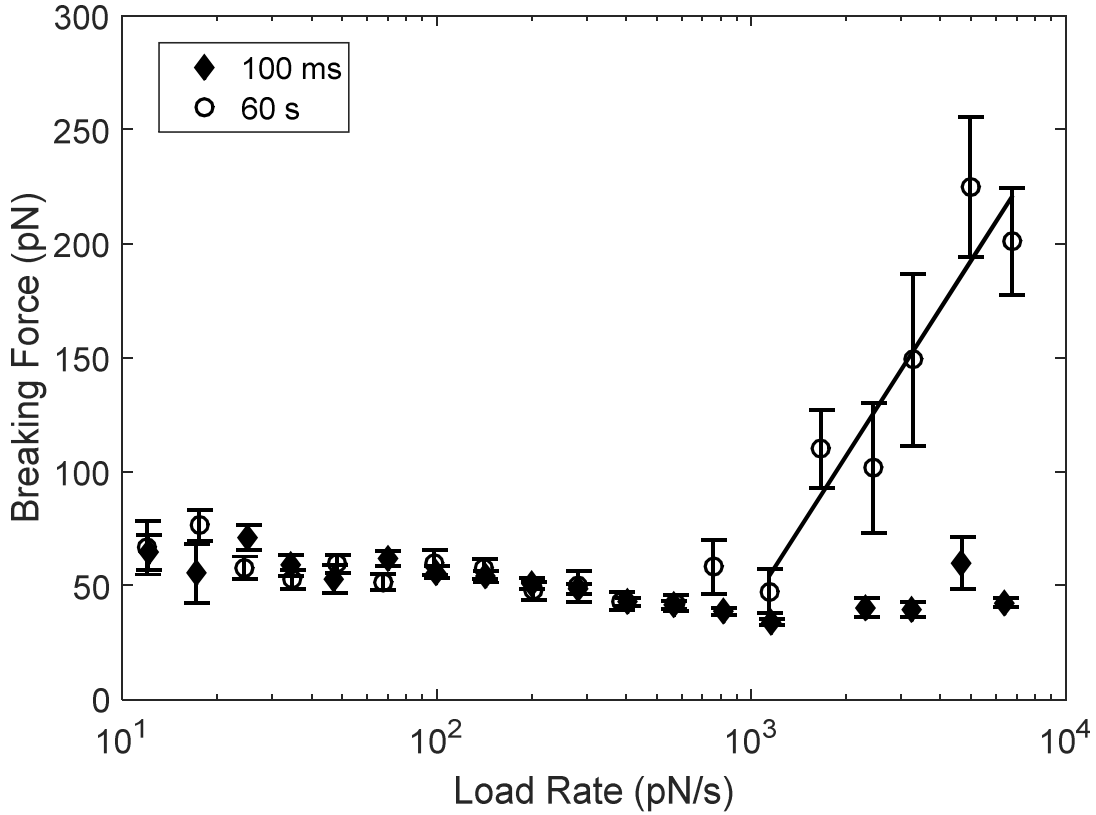
Figure 19. Bond dissociation forces as a function of loading rate measured on a 65 kPa polyacrylamide gel. 100 ms contact time (solid diamonds) and 60s contact time (open circles). At roughly 10^3 pN/s there is a transition to the loading-dependent regime. The solid line represents a fit to the Bell model.

From the loading-dependent regime, it is possible to extract the bond parameters, x_b and v_0, described by Bell's model. The original model,

$$F_d = \frac{k_B T}{x_b} \ln\left(\frac{x_b}{v_0 k_B T} r\right),$$

can be simplified to fit the form

$$F_d = a \ln(r) + b,$$

where we have made the substitutions

$$a = \frac{k_B T}{x_b} \qquad \text{and} \qquad b = a \ln\left(\frac{1}{v_0 a}\right).$$

By performing a least-squares fit of this function to the experimental data above the 500 pN/s threshold, we have extracted the parameters x_b, representing the bond's potential energy barrier

38

half-width, and ν_0, representing the bond's intrinsic dissociation rate. These parameters are shown as a function of gel stiffness in **Figure 20**. The fact that these values are dependent upon the substrate stiffness is an indication that the integrin undergoes conformational changes that alter the molecule's binding affinity for collagen in a stiffness-dependent manner.
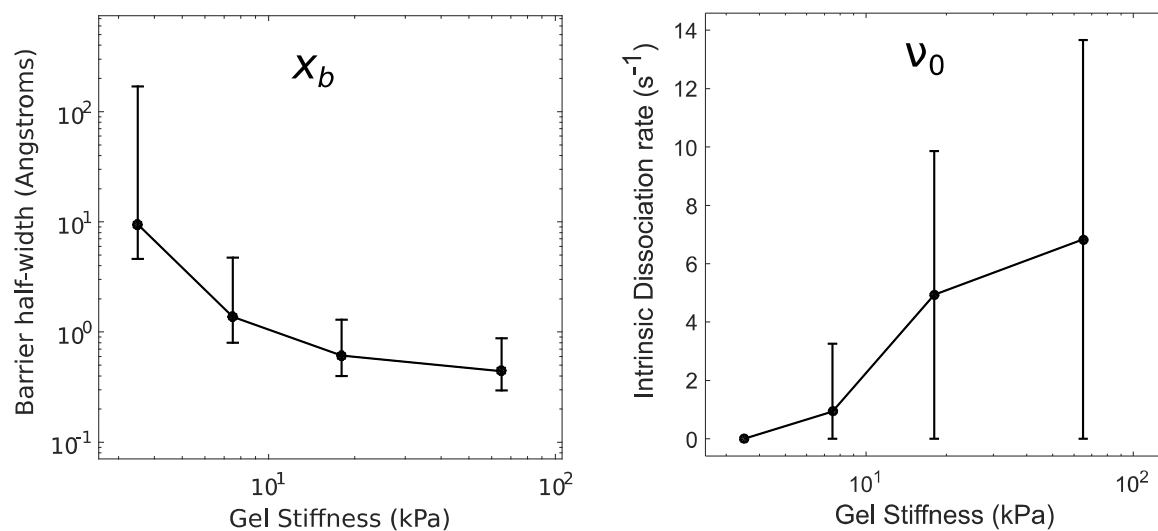
Figure 20. Bond parameters. x_b (width of the potential barrier), and ν_0 (intrinsic dissociation rate), as a function of the substrate stiffness. Error bars represent the 95% confidence intervals of the fitting parameters.

Discussion

Effect of Substrate Stiffness on integrin activation

Within the last year, a study by Jiang et al. reported a slight increase in integrin-ligand unbinding force between DGEA-coated PDMS substrates of 500 Pa (neurogenic stiffness) and 1×10^5 Pa (osteogenic) [85]. This result affirms that although the binding affinity of integrins to ECM ligands is affected by the mechanical stiffness of the substrate, the effect is small and requires stiffness changes of several orders of magnitude before any single-molecule strengthening becomes apparent. In the present study we observed no significant change in molecular binding strength between gels, due to the small range of gel stiffness that were tested.

Nevertheless, we observed loading-dependent bond strengthening in SCFS measurements, consistent with Bell's model, both on the control (glass) substrate and the polyacrylamide gels. While the series-spring model of cell-ECM interaction (as discussed in Chapter 2) lays out a clear mechanism for the ECM stiffness to modulate the loading of the bonds, it is likely that this small dependence is overshadowed by the reorganization and clustering of integrins, which is also stiffness-dependent.

Effect of substrate stiffness on bond clustering

While the single-bond peak rupture force increased slightly with hydrogel stiffness, the rupture force distribution of the stiffer gels (45-65 kPa) was also characterized by the appearance of very large (100-400 pN) rupture forces (~22% of events on 65kPa gel were greater than 100 pN, vs. 10% of events on 3.5 kPa). This range of forces is substantially higher than reported values for single-molecule unbinding events, and is therefore likely to indicate that the ruptured adhesions consisted of multiple integrin-ligand bonds clustered together. These large-force rupture events occurred rarely on the softer hydrogels, suggesting that stiff substrates play a role in promoting a higher degree of integrin clustering which leads to the higher observed rupture forces.

A computational study by Paszek et al. [82] established a model showing the effect of matrix stiffness on integrin clustering. By considering the range of movement of ligands bound to a flexible substrate, the simulation concluded that a highly flexible extracellular matrix allows for more rapid association between integrins and ligands – regardless of their proximity to existing bonds. In contrast, the probability of an integrin binding to stiff matrix ligands increases sharply only in regions close to existing bonds, leading to bond clustering. The result is that cells are able

to form nascent adhesions more rapidly on soft substrates, but that those small adhesions only form readily into focal complexes on a stiff substrate. It is suggested that this could be one way in which the matrix stiffness regulates cellular adhesion and tension. Our results confirm this result, showing that in the short contact regime (0.1 s) the bonds form more rapidly on soft gels than stiff gels (**Figure 16**), but the total number of bonds at longer times is not affected by stiffness.

Our current understanding of the cell-substrate attachment process is illustrated in **Figure 21**. Within the cytoplasm, actin filaments bind to the integrins by way of adapter proteins, including talin and vinculin, while in the extracellular space integrins bind to the ligands present in the ECM. Following the initial integrin-ligand attachment, the integrins undergo a conformational change ("activation") leading to the formation of a catch bond which increases in strength under loading. Finally, additional integrins diffuse along the cell membrane and bind near the site of initial attachments to form stronger focal adhesion complexes. This clustering of integrins becomes more favorable as matrix stiffness increases.

The focal adhesions are dynamic complexes in which integrins continually bind and unbind to maintain the cytoskeletal tension [24]. Prior research has concluded that the tensile force applied by cells is regulated by the number of bound integrins, as well as the degree of integrin clustering. In the present study, we observe that although the change in integrin-ligand dissociation force was not significant between different gels, there is strong evidence to suggest that the energy landscape is in some way affected by ECM stiffness and therefore the bond dynamics may also play a role in regulating cytoskeletal tension.

Because the substrate stiffness has the ability to regulate the individual bond activation and not only integrin clustering, it is likely that cells make use of this effect to probe the stiffness of their ECM. By sensing changes in the turnover rate of bonds within the dynamic focal complexes, cells may mechanically detect changes in the ECM stiffness.
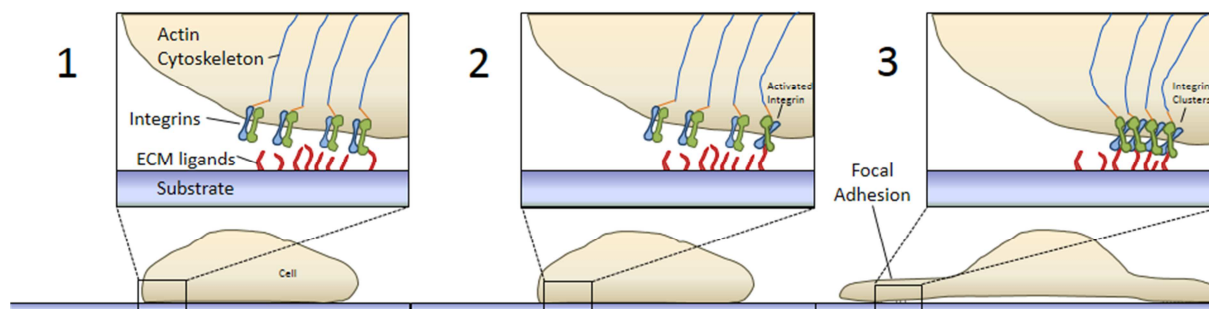
Figure 21. Initial stages of cell attachment. Cell attachment begins with inactive integrins binding weakly to ECM (1), followed by integrin activation (2), and then recruitment of additional integrins to form clusters (3). Overall adhesion strength is dependent both upon clustering and the individual integrin-ligand bond strength.

Limitations

Although collagen-coated polyacrylamide gels strive to create a crude imitation of extracellular matrix, it would be naïve to assume that the environmental conditions during the AFM experiment are identical to those experienced by a cell embedded in a tissue. The experimental substrates were coated with only a controlled concentration of collagen, whereas native ECM is likely to contain a wide selection of ligands with varying density. Furthermore, the AFM pulling experiment applies a controlled retraction velocity which is dissimilar to *in-vivo* loading. The most common sources of bond loading *in-vivo* are the retrograde flow of actin and the activity of myosin II, both of which may vary widely in velocity depending on the cell's shape, migratory patterns, and external conditions. Additionally, the time of contact between the cell and substrate was fixed at 0.1 or 60 s during the experiment, whereas the integrin-ligand bonds may persist for much longer in a native environment.

The measurements presented here were taken from a minimum of 100 force-distance curves and 3 cells per sample condition. The time-consuming nature of measurements and data processing proved to be a limiting factor in the amount of data that could be acquired. Due to the inherent heterogeneity of cell populations, it is likely that random variations between cells (integrin density, cytoskeletal structure, mitotic phase, other non-α2β1 integrin binding, and numerous other factors) as well as nonspecific binding contribute significantly to the statistical noise in our measurements. With additional time and resources, the statistics could be improved, potentially to the point of uncovering significant changes in bond strength, even over a small biologically-relevant range of substrate stiffness.

Chapter 5 – Conclusions

In Chapter 3, we developed a reliable method to measure the stiffness of cells cultured on different substrates. Using this method we have shown that tissue cells exhibit changes in morphology and stiffness as a result of changing stiffness of their surroundings. Subsequently, in Chapter 4, we investigated how this regulation of cell stiffness is driven by the influence of the substrate stiffness on the dynamics of integrin-mediated adhesions between the cell and the extracellular material.

Two major mechanisms exist for integrin-mediated stiffness sensing. The primary mechanism, which acts over long time scales (~10 min), is the formation of integrin clusters [8, 15-19, 22, 24, 25]. On stiff surfaces, integrins are more likely to bind close to existing adhesion sites, leading to closely clustered bonds which become the sites of focal complexes that mature into focal adhesions. On compliant surfaces, the integrins can bind to ECM easily without clustering, resulting in cells that migrate faster, spread less, and are more compliant than cells on stiff surfaces.

The secondary mechanism which acts on short time scales (~1 min) is the integrin activation. Integrins themselves can act as force transducers, by modulating their binding affinity in response to applied tension. An external tension applied to the integrin molecule leads to conformational changes which reveal or conceal binding sites, leading to integrin activation and increased binding affinity.

Because the molecular dissociation is a stochastic process dependent upon an intrinsic off-rate as well as the applied external force, the bond strength depends not only upon the applied force but also the timescale of loading. At fast loading rates, the integrin-ligand bonds exhibit shorter lifetimes but higher dissociation forces, allowing the cell to sustain a higher cytoskeletal tension. This effect combines with the changes in integrin clustering affinity to produce significant changes in cell morphology, migration, spreading area, and stiffness as a result of changes in ECM stiffness.

Integrins are a single component of a complex pathway for force transduction within the cell. It is not only possible but likely that other components, such as the adapter proteins, actin filaments, and microtubules, play a role in modulating the cytoskeletal tension and structure in

response to external stimuli. By investigating the integrins' behavior in response to changes in ECM stiffness, we have contributed to a growing field of research in cellular transduction of mechanical forces.

Appendices

Appendix A: Monte-Carlo Simulation

Motivation

A Monte-Carlo type simulation was created and run using MATLAB to demonstrate the validity of applying Bell's model to our experimental data. In essence, the same AFM pulling experiment was simulated using the mechanics and rupture probability described by the Bell model, and the rupture force was averaged over multiple runs to be compared with experimental results.

To execute this simulation, it was necessary to assume certain values of the physical parameters, including barrier width (Δx), diffusion coefficient (D), pulling velocity (v), and base dissociation rate (v_0), as well as simulation parameters including the stiffness of the substrate (k_s), cell (k_{cell}), and cantilever (k_{tip}), and the timestep (Δt). A full list of parameters, along with the complete MATLAB code for the simulation, is provided at the end.

Procedure

The procedure for each timestep of the pulling experiment is as follows:

1. Assuming constant velocity plus Brownian displacement (starting at $t = 0$), compute the net displacement of the system,

$$\Delta z = v \cdot \Delta t + D \cdot randn(1)$$

where randn selects a value at random from a normal distribution centered about 0 with a variance of 1.

2. Add this displacement to the previous position to find the total displacement

$$z(t) = z(t - \Delta t) + \Delta z$$

3. From this displacement, compute the total tension of the system:

$$F = z \cdot \cfrac{1}{{}^{1}\!/\!{k_{tip}} + {}^{1}\!/\!{k_{cell}} + {}^{1}\!/\!{k_{s}}}$$

4. Compute the force-dependent off rate,

$$v(t) = v_0 \exp\left(\frac{F(t)x_b}{k_B T}\right)$$

and the bond rupture probability for the current timestep

$$P(t, \Delta t) = 1 - \exp(-v(t)\Delta t)$$

5. Generate a random number n between 0 and 1.

6. If $n > P$, advance to the next timestep. If not, the bond is considered broken and the current force is recorded as the rupture force, and loading rate is taken as the slope of the curve during the last 100 ms of loading.

Results

The results of the simulation were binned by loading rate and plotted in the same manner as in the AFM experiment. Results are shown in **Figure 22**. A clear transition is visible around 10^3 pN/s from the loading-independent to the loading-dependent regime.
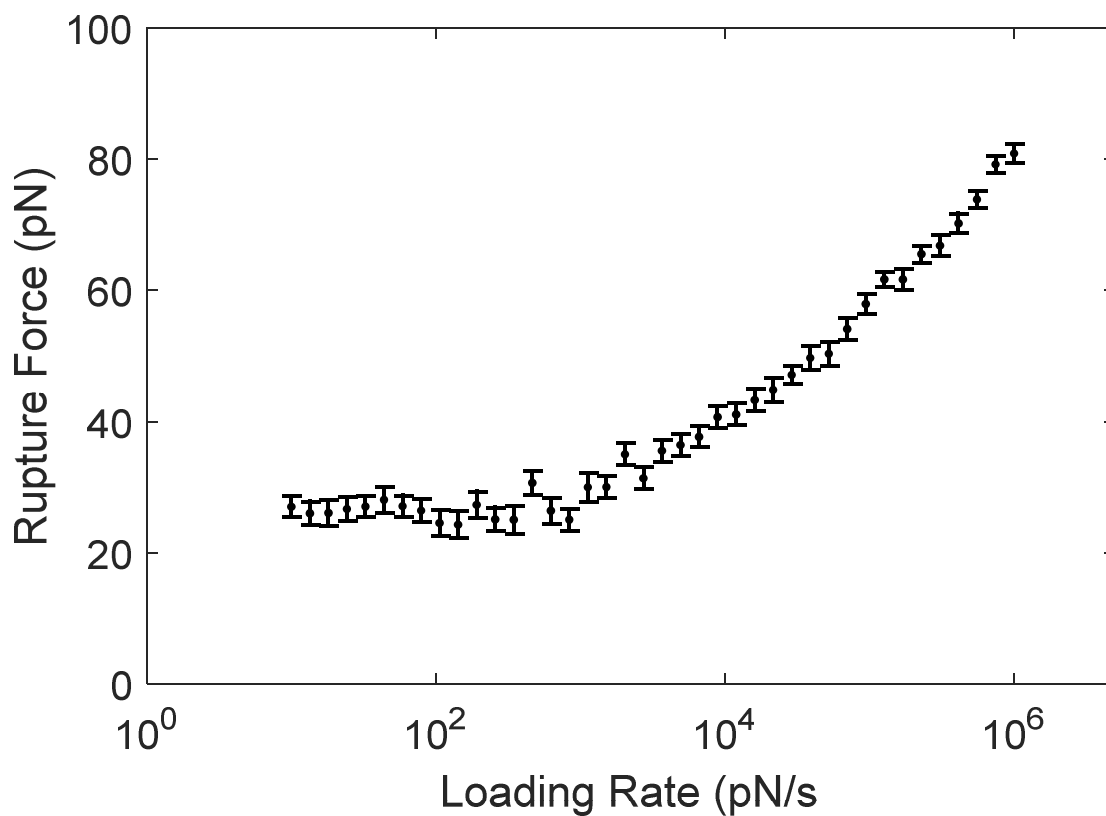
Figure 22. Simulated bond dissociation force as a function of loading rate.

To test the original hypothesis that the breaking force is dependent on substrate stiffness, the simulation was run with ks = 0.00001, 0.0001, 0.001, 0.01, 0.1, and 1 N/m, with 50 iterations for each condition. The breaking force increased logarithmically with substrate stiffness, with mean values ranging from 10-80 pN as shown in **Figure 23**.

47
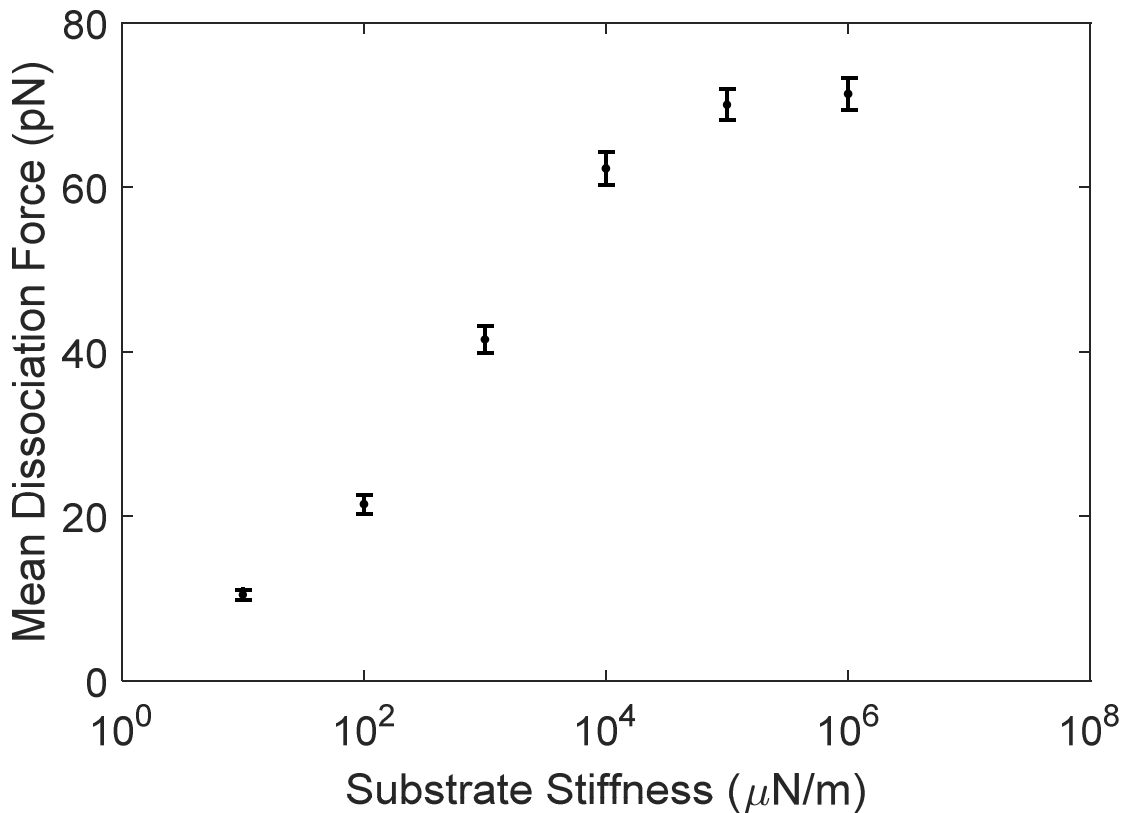
Figure 23. Simulated bond dissociation force as a function of substrate stiffness.

Discussion

By means of a stochastic simulation based on the Bell model, we have reproduced the results generated by Evans and Ritchie [38] which showed the transition from random, independent dissociations to a loading-dependent regime of bond strengthening. Furthermore, we have verified that a relationship exists between ECM stiffness and the individual integrin-ligand binding strength. However, the large range stiffness required to produce a significant change in bond strength extends beyond the stiffness of materials that are commonly found *in-vivo*, suggesting that this effect plays a small role in mechanotransduction compared to other mechanisms such as integrin clustering.

When executing the Monte-Carlo simulation, several assumptions were made that are not necessarily realistic. The simulation only treated a single bond at a time, and did not account for the possibility of multiple or cooperative binding, as was observed in the experiment. A more

robust simulation would include the probability of bond clustering, as well as modifications to the energy landscape in the event that multiple integrins were bound to the same collagen molecule.

The simulation was written under the assumption that Bell's model is universally applicable, without restriction to the values of k_off or force that were computed. Superficially, this appears to be acceptable, with the caveat that our simulation did not reproduce the bond strength plateau described in [38]. This plateau occurs as the result of the kinetic breakdown of the bond under ultrafast loading, which is not accounted for in Bell's model.

Simulation Parameters

The following values were assumed during the simulation shown in **Table 4**. These values were estimated based on a survey of values reported in the literature [72, 73, 86, 87].

Parameter Name	Description	Value
D	1-D diffusion coefficient	$5 \times 10^{-6} \text{m}^2/\text{s}$
$k_B T$	Thermal energy	$4 \times 10^{-21} \text{J}$
ν_0	Intrinsic bond dissociation rate	0.1 s^{-1}
x_b	Barrier half-width	1 Å

Table 4. Parameters used during the Monte-Carlo simulation.

MATLAB Code

Below is the entire MATLAB code used to run the simulation. This code makes use of the MATLAB Parallel Processing toolbox command `parfor;` however, if the Parallel Processing toolbox is unavailable this may be replaced by a standard `for` loop, with reduced performance.

```matlab
clear all
close all

N = 50;

%constants
kc = 0.6;
kss = [0.00001 0.0001 0.001 0.01 0.1 1];
kcell = 0.01;

D = 5e-6;
kBT = 4.14e-21;
v0 =  0.1;
xb = 1e-10;
vel = logspace(-9,-4,40);
zc = 1e-12;
timestep = 1e-5;

rng('shuffle')

%these are the sample condition loops
for k = 1:length(kss)
ks = kss(k);
maxforce{k} = zeros(numel(vel),N);
loadingrate{k} = zeros(numel(vel),N);
lifetime{k} = zeros(numel(vel),N);


for j = 1:numel(vel)
keff = 1/(1/kc + 1/ks + 1/kcell);
v = vel(j);

%this is the iteration loop
parfor i = 1:N
disp(['condition ', num2str(j), ', iteration ', num2str(i)])
%initialize values
t = 0;
z=50e-12;
zpos = z;
broken = false;
F = 1e-12;
Force = zeros(1,100000000);
step = 0;
```

```matlab
%this is the actual simulation
while broken == false;
    t = t+timestep; %advance time
    step = step+1; %advance step
    brw = D * randn * timestep; %brownian displacement
    zdisp = v*timestep + brw; %total displacement
    z = z + zdisp;
    F = z*keff; %compute force
    Force(step) = F;
    Nd = 1-exp(v0*exp(F*xb/kBT)*timestep);

    %reset Force if it gets too long
    if step > 99999999
        Force(1:100000) = Force(99900000:99999999);
        step = 100000;
    end



    %check if broken
    if rand < Nd
        broken = true;
        mf(i) = F;
        lr(i) = mean(diff(Force(max([1 step-100000]):step)))/timestep;
        lt(i) = t;
    end

end

end
maxforce{k}(j,:) = mf;
loadingrate{k}(j,:) = lr;
lifetime{k}(j,:) = lt;
favg{k}(j) = mean(mf);
lavg{k}(j) = mean(lr);
fstd{k}(j) = std(mf)/sqrt(numel(mf));
lstd{k}(j) = std(lr)/sqrt(numel(lr));
end
end
save(['simdata_' datestr(now,30) '.mat'], 'maxforce', 'loadingrate','vel',
'lifetime', 'favg', 'lavg', 'fstd', 'lstd');
```

References

1.   Georges, P.C. and P.A. Janmey, *Cell type-specific response to growth on soft materials.* Journal of Applied Physiology, 2005. **98**(4): p. 1547-1553.
2.   Thomas, G., et al., *Measuring the Mechanical Properties of Living Cells Using Atomic Force Microscopy.* J. Vis. Exp, 2013(76): p. e50497.
3.   Yeung, T., et al., *Effects of substrate stiffness on cell morphology, cytoskeletal structure, and adhesion.* Cell Motility and the Cytoskeleton, 2005. **60**(1): p. 24-34.
4.   Suresh, S., *Biomechanics and biophysics of cancer cells.* Acta Biomaterialia, 2007. **3**(4): p. 413-438.
5.   Kumar, S. and V. Weaver, *Mechanics, malignancy, and metastasis: The force journey of a tumor cell.* Cancer and Metastasis Reviews, 2009. **28**(1-2): p. 113-127.
6.   Huang, J.Y., et al., *Influence of substrate stiffness on cell-substrate interfacial adhesion and spreading: A mechano-chemical coupling model.* Journal of Colloid and Interface Science, 2011. **355**(2): p. 503-508.
7.   Girard, P.P., et al., *Cellular chemomechanics at interfaces: sensing, integration and response.* Soft Matter, 2007. **3**: p. 307 - 326.
8.   Discher, D.E., P. Janmey, and Y.-l. Wang, *Tissue cells feel and respond to the stiffness of their substrate.* Science (Washington, DC, U. S.), 2005. **310**(5751): p. 1139 - 1143.
9.   Abbott, A., *Cell culture: Biology's new dimension.* Nature (London, U. K.), 2003. **424**: p. 870 - 872.
10.   Tyska, M.J. and D.M. Warshaw, *The myosin power stroke.* Cell Motil Cytoskeleton, 2002. **51**(1): p. 1-15.
11.   Schlaepfer, D.D., et al., *Integrin-Mediated Signal-Transduction Linked to Ras Pathway by Grb2 Binding to Focal Adhesion Kinase.* Nature, 1994. **372**(6508): p. 786-791.
12.   Critchley, D.R., et al., *Integrin-mediated cell adhesion: the cytoskeletal connection.* Cell Behaviour: Control and Mechanism of Motility, 1999(65): p. 79-99.
13.   Cary, L.A., D.C. Han, and J.L. Guan, *Mechanism of signal transduction by focal adhesion kinase in integrin-mediated cell migration.* Molecular Biology of the Cell, 1997. **8**: p. 2323-2323.
14.   Chan, C.E. and D.J. Odde, *Traction Dynamics of Filopodia on Compliant Substrates.* Science, 2008. **322**(5908): p. 1687-1691.
15.   Katsumi, A., et al., *Integrins in mechanotransduction.* Journal of Biological Chemistry, 2004. **279**(13): p. 12001-12004.
16.   Pedersen, J.A. and M.A. Swartz, *Mechanobiology in the third dimension.* Annals of Biomedical Engineering, 2005. **33**(11): p. 1469-1490.
17.   Paszek, M.J., et al., *Tensional homeostasis and the malignant phenotype.* Cancer Cell, 2005. **8**(3): p. 241-254.
18.   Luo, B.H., C.V. Carman, and T.A. Springer, *Structural basis of integrin regulation and signaling.* Annual Review of Immunology, 2007. **25**: p. 619-647.
19.   Humphries, J.D., A. Byron, and M.J. Humphries, *Integrin ligands at a glance.* Journal of Cell Science, 2006. **119**(19): p. 3901-3903.
20.   Zhang, Z.G., et al., *Effects of constitutively active GTPases on fibroblast behavior.* Cellular and Molecular Life Sciences, 2006. **63**(1): p. 82-91.
21.   Jokinen, J., et al., *Integrin-mediated cell adhesion to type I collagen fibrils.* J Biol Chem, 2004. **279**(30): p. 31956-63.
22.   Wang, N., J.P. Butler, and D.E. Ingber, *Mechanotransduction across the Cell-Surface and through the Cytoskeleton.* Science, 1993. **260**(5111): p. 1124-1127.
23.   Zolkiewska, A., *Ecto-ADP-ribose transferases: Cell-surface response to local tissue injury.* Physiology, 2005. **20**: p. 374-381.

24.   Bershadsky, A., M. Kozlov, and B. Geiger, *Adhesion-mediated mechanosensitivity: a time to experiment, and a time to theorize.* Current Opinion in Cell Biology, 2006. **18**(5): p. 472-481.

25.   Geiger, B. and A. Bershadsky, *Assembly and mechanosensory function of focal contacts.* Current Opinion in Cell Biology, 2001. **13**(5): p. 584-592.

26.   Humphries, J.D., et al., *Vinculin controls focal adhesion formation by direct interactions with talin and actin.* J Cell Biol, 2007. **179**(5): p. 1043-57.

27.   Geiger, B., et al., *Transmembrane extracellular matrix-cytoskeleton crosstalk.* Nature Reviews Molecular Cell Biology, 2001. **2**(11): p. 793-805.

28.   Lee, S.E., R.D. Kamm, and M.R.K. Mofrad, *Force-induced activation of Talin and its possible role in focal adhesion mechanotransduction.* Journal of Biomechanics, 2007. **40**(9): p. 2096-2106.

29.   del Rio, A., et al., *Stretching Single Talin Rod Molecules Activates Vinculin Binding.* Science, 2009. **323**(5914): p. 638-641.

30.   Nobes, C.D. and A. Hall, *Rho, Rac, and Cdc42 Gtpases Regulate the Assembly of Multimolecular Focal Complexes Associated with Actin Stress Fibers, Lamellipodia, and Filopodia.* Cell, 1995. **81**(1): p. 53-62.

31.   Riveline, D., et al., *Focal contacts as mechanosensors: Externally applied local mechanical force induces growth of focal contacts by an mDia1-dependent and ROCK-independent mechanism.* Journal of Cell Biology, 2001. **153**(6): p. 1175-1185.

32.   Pelham, R.J. and Y.L. Wang, *Cell locomotion and focal adhesions are regulated by substrate flexibility.* Proceedings of the National Academy of Sciences of the United States of America, 1997. **94**(25): p. 13661-13665.

33.   Nicolas, A., A. Besser, and S.A. Safran, *Dynamics of cellular focal adhesions on deformable substrates: Consequences for cell force microscopy.* Biophysical Journal, 2008. **95**(2): p. 527-539.

34.   Bell, G.I., *Theoretical-Models for the Specific Adhesion of Cells to Cells or to Surfaces.* Advances in Applied Probability, 1980. **12**(3): p. 566-567.

35.   Lele, T.P., et al., *Mechanical forces alter zyxin unbinding kinetics within focal adhesions of living cells.* Journal of Cellular Physiology, 2006. **207**(1): p. 187-194.

36.   Dembo, M., et al., *The Reaction-Limited Kinetics of Membrane-to-Surface Adhesion and Detachment.* Proceedings of the Royal Society Series B-Biological Sciences, 1988. **234**(1274): p. 55-83.

37.   Kong, F., et al., *Demonstration of catch bonds between an integrin and its ligand.* Journal of Cell Biology, 2009. **185**(7): p. 1275-1284.

38.   Evans, E. and K. Ritchie, *Dynamic strength of molecular adhesion bonds.* Biophys J, 1997. **72**(4): p. 1541-55.

39.   He, S.J., et al., *Some basic questions on mechanosensing in cell-substrate interaction.* Journal of the Mechanics and Physics of Solids, 2014. **70**: p. 116-135.

40.   Ziebert, F. and I.S. Aranson, *Effects of Adhesion Dynamics and Substrate Compliance on the Shape and Motility of Crawling Cells.* Plos One, 2013. **8**(5).

41.   Hoffman, B.D. and J.C. Crocker, *Cell mechanics: dissecting the physical responses of cells to force.* Annu Rev Biomed Eng, 2009. **11**: p. 259-88.

42.   Hoffman, B.D., et al., *The consensus mechanics of cultured mammalian cells.* Proc Natl Acad Sci U S A, 2006. **103**(27): p. 10259-64.

43.   Lau, A.W., et al., *Microrheology, stress fluctuations, and active behavior of living cells.* Phys Rev Lett, 2003. **91**(19): p. 198101.

44.   Liu, J., et al., *Microrheology probes length scale dependent rheology.* Phys Rev Lett, 2006. **96**(11): p. 118104.

45.   Deng, L., et al., *Fast and slow dynamics of the cytoskeleton.* Nat Mater, 2006. **5**(8): p. 636-40.

46.   Oh, M.J., et al., *Micropipette Aspiration of Substrate-attached Cells to Estimate Cell Stiffness.* J Vis Exp, 2012. **67**: p. e3886.

47.   Levental, I., et al., *A simple indentation device for measuring micrometer-scale tissue stiffness.* Journal of Physics-Condensed Matter, 2010. **22**(19).

48.   Mahaffy, R.E., et al., *Quantitative analysis of the viscoelastic properties of thin regions of fibroblasts using atomic force microscopy.* Biophys J, 2004. **86**(3): p. 1777-93.

49.   Radmacher, M., *Measuring the elastic properties of biological samples with the AFM.* IEEE Eng Med Biol Mag, 1997. **16**(2): p. 47-57.

50.   Crocker, J.C. and B.D. Hoffman, *Multiple-particle tracking and two-point microrheology in cells.* Methods Cell Biol, 2007. **83**: p. 141-78.

51.   Liu, F. and D.J. Tschumperlin, *Micro-mechanical characterization of lung tissue using atomic force microscopy.* J Vis Exp, 2011(54).

52.   Solon, J., et al., *Fibroblast adaptation and stiffness matching to soft elastic substrates.* Biophys J, 2007. **93**(12): p. 4453-61.

53.   Wu, H.W., T. Kuhn, and V.T. Moy, *Mechanical properties of l929 cells measured by atomic force microscopy: Effects of anticytoskeletal drugs and membrane crosslinking.* Scanning, 1998. **20**(5): p. 389-397.

54.   Radmacher, M., et al., *Measuring the viscoelastic properties of human platelets with the atomic force microscope.* Biophys J, 1996. **70**(1): p. 556-67.

55.   Burnham, N.A., et al., *Comparison of calibration methods for atomic-force microscopy cantilevers.* Nanotechnology, 2003. **14**(1): p. 1.

56.   Davis, J.T., et al., *Muller cell expression of genes implicated in proliferative vitreoretinopathy is influenced by substrate elastic modulus.* Invest Ophthalmol Vis Sci, 2012. **53**(6): p. 3014-9.

57.   A-Hassan, E., et al., *Relative microelastic mapping of living cells by atomic force microscopy.* Biophysical Journal, 1998. **74**(3): p. 1564-1578.

58.   Costa, K.D., A.J. Sim, and F.C. Yin, *Non-Hertzian approach to analyzing mechanical properties of endothelial cells probed by atomic force microscopy.* J Biomech Eng, 2006. **128**(2): p. 176-84.

59.   Xiong, Y., et al., *Topography and nanomechanics of live neuronal growth cones analyzed by atomic force microscopy.* Biophys J, 2009. **96**(12): p. 5060-72.

60.   Byfield, F.J., et al., *Absence of filamin A prevents cells from responding to stiffness gradients on gels coated with collagen but not fibronectin.* Biophys J, 2009. **96**(12): p. 5095-102.

61.   Cross, S.E., et al., *AFM-based analysis of human metastatic cancer cells.* Nanotechnology, 2008. **19**(38): p. 384003.

62.   Engler, A.J., et al., *Microtissue elasticity: Measurements by atomic force microscopy and its influence on cell differentiation.* Cell Mechanics, 2007. **83**: p. 521-+.

63.   Lin, D.C., E.K. Dimitriadis, and F. Horkay, *Robust strategies for automated AFM force curve analysis--I. Non-adhesive indentation of soft, inhomogeneous materials.* J Biomech Eng, 2007. **129**(3): p. 430-40.

64.   Storm, C., et al., *Nonlinear elasticity in biological gels.* Nature, 2005. **435**(7039): p. 191-4.

65.   Wen, Q. and P.A. Janmey, *Polymer physics of the cytoskeleton.* Curr Opin Solid State Mater Sci, 2011. **15**(5): p. 177-182.

66.   Stilwell, N.A. and D. Tabor, *Elastic Recovery of Conical Indentations.* Proceedings of the Physical Society, 1961. **78**(2): p. 169.

67.   Vinckier, A. and G. Semenza, *Measuring elasticity of biological materials by atomic force microscopy.* FEBS Letters, 1998. **430**(1–2): p. 12-16.

68.   Vinckier, A., et al., *Dynamical and mechanical study of immobilized microtubules with atomic force microscopy.* Journal of Vacuum Science and Technology B: Microelectronics and Nanometer Structures, 1996. **14**(2): p. 1427-1431.

69.   Dimitriadis, E.K., et al., *Determination of elastic moduli of thin layers of soft material using the atomic force microscope.* Biophys J, 2002. **82**(5): p. 2798-810.

70.   Oliver, W.C. and G.M. Pharr, *An Improved Technique for Determining Hardness and Elastic-Modulus Using Load and Displacement Sensing Indentation Experiments.* Journal of Materials Research, 1992. **7**(6): p. 1564-1583.

71.   Li, F.Y., et al., *Force measurements of the alpha(5)beta(1) integrin-fibronectin interaction.* Biophysical Journal, 2003. **84**(2): p. 1252-1262.

72.   Taubenberger, A., et al., *Revealing early steps of alpha(2)beta(1) integrin-mediated adhesion to collagen type I by using single-cell force spectroscopy.* Molecular Biology of the Cell, 2007. **18**(5): p. 1634-1644.

73.   Franz, C.M., et al., *Studying integrin-mediated cell adhesion at the single-molecule level using AFM force spectroscopy.* Sci STKE, 2007. **2007**(406): p. pl5.

74.   Friedrichs, J., et al., *A practical guide to quantify cell adhesion using single-cell force spectroscopy.* Methods, 2013. **60**(2): p. 169-178.

75.   Wang, Y.L. and R.J. Pelham, *Preparation of a flexible, porous polyacrylamide substrate for mechanical studies of cultured cells.* Molecular Motors and the Cytoskeleton, Pt B, 1998. **298**: p. 489-496.

76.   Zhang, X.H., E. Wojcikiewicz, and V.T. Moy, *Force spectroscopy of the leukocyte function-associated antigen-1/intercellular adhesion molecule-1 interaction.* Biophysical Journal, 2002. **83**(4): p. 2270-2279.

77.   Du, J., et al., *Integrin activation and internalization on soft ECM as a mechanism of induction of stem cell differentiation by ECM elasticity.* Proceedings of the National Academy of Sciences of the United States of America, 2011. **108**(23): p. 9466-9471.

78.   Friedland, J.C., M.H. Lee, and D. Boettiger, *Mechanically activated integrin switch controls alpha5beta1 function.* Science, 2009. **323**(5914): p. 642-4.

79.   Gallant, N.D., K.E. Michael, and A.J. Garcia, *Cell adhesion strengthening: Contributions of adhesive area, integrin binding, and focal adhesion assembly.* Molecular Biology of the Cell, 2005. **16**(9): p. 4329-4340.

80.   Helenius, J., et al., *Single-cell force spectroscopy.* Journal of Cell Science, 2008. **121**(11): p. 1785-1791.

81.   Opfer, J. and K.E. Gottschalk, *Identifying Discrete States of a Biological System Using a Novel Step Detection Algorithm.* Plos One, 2012. **7**(11).

82.   Paszek, M.J., et al., *Integrin clustering is driven by mechanical resistance from the glycocalyx and the substrate.* PLoS Comput Biol, 2009. **5**(12): p. e1000604.

83.   Nordin, D., L. Donlon, and D. Frankel, *Characterising single fibronectin-integrin complexes.* Soft Matter, 2012. **8**(22): p. 6151-6160.

84.   Barczyk, M., S. Carracedo, and D. Gullberg, *Integrins.* Cell Tissue Res, 2010. **339**(1): p. 269-80.

85.   Jiang, L., et al., *Cells Sensing Mechanical Cues: Stiffness Influences the Lifetime of Cell-Extracellular Matrix Interactions by Affecting the Loading Rate.* Acs Nano, 2016. **10**(1): p. 207-217.

86.   Gupta, V.K., *Stochastic simulation of single-molecule pulling experiments.* Eur Phys J E Soft Matter, 2014. **37**(10): p. 99.

87.   Qian, J., et al., *Lifetime and Strength of Periodic Bond Clusters between Elastic Media under Inclined Loading.* Biophysical Journal, 2009. **97**(9): p. 2438-2445.